RESEARCH ARTICLE

CDK4/6 Inhibition Augments Antitumor Immunity by Enhancing T-cell Activation

Jiehui Deng[1,2], Eric S. Wang[3], Russell W. Jenkins[1,4], Shuai Li[1], Ruben Dries[1,5], Kathleen Yates[6], Sandeep Chhabra[3], Wei Huang[1,6], Hongye Liu[1,7], Amir R. Aref[1,7], Elena Ivanova[1,7], Cloud P. Paweletz[1,7], Michaela Bowden[1,8], Chensheng W. Zhou[1,8], Grit S. Herter-Sprie[1], Jessica A. Sorrentino[9], John E. Bisi[9], Patrick H. Lizotte[1,7], Ashley A. Merlino[1], Max M. Quinn[1], Lauren E. Bufe[1], Annan Yang[1], Yanxi Zhang[1], Hua Zhang[1], Peng Gao[1], Ting Chen[1], Megan E. Cavanaugh[1,7], Amanda J. Rode[1,7], Eric Haines[1], Patrick J. Roberts[9], Jay C. Strum[9], William G. Richards[10], Jochen H. Lorch[1], Sareh Parangi[11], Viswanath Gunda[11], Genevieve M. Boland[11], Raphael Bueno[10], Sangeetha Palakurthi[1,7], Gordon J. Freeman[1,12], Jerome Ritz[13], W. Nicholas Haining[6], Norman E. Sharpless[14], Haribabu Arthanari[3], Geoffrey I. Shapiro[1,12], David A. Barbie[1,12], Nathanael S. Gray[3], and Kwok-Kin Wong[1,2,7,12]

ABSTRACT Immune checkpoint blockade, exemplified by antibodies targeting the PD-1 receptor, can induce durable tumor regressions in some patients. To enhance the efficacy of existing immunotherapies, we screened for small molecules capable of increasing the activity of T cells suppressed by PD-1. Here, we show that short-term exposure to small-molecule inhibitors of cyclin-dependent kinases 4 and 6 (CDK4/6) significantly enhances T-cell activation, contributing to antitumor effects *in vivo*, due in part to the derepression of NFAT family proteins and their target genes, critical regulators of T-cell function. Although CDK4/6 inhibitors decrease T-cell proliferation, they increase tumor infiltration and activation of effector T cells. Moreover, CDK4/6 inhibition augments the response to PD-1 blockade in a novel *ex vivo* organotypic tumor spheroid culture system and in multiple *in vivo* murine syngeneic models, thereby providing a rationale for combining CDK4/6 inhibitors and immunotherapies.

SIGNIFICANCE: Our results define previously unrecognized immunomodulatory functions of CDK4/6 and suggest that combining CDK4/6 inhibitors with immune checkpoint blockade may increase treatment efficacy in patients. Furthermore, our study highlights the critical importance of identifying complementary strategies to improve the efficacy of immunotherapy for patients with cancer. *Cancer Discov; 8(2); 216–33. ©2017 AACR.*

See related commentary by Balko and Sosman, p. 143.
See related article by Jenkins et al., p. 196.

INTRODUCTION

Immunotherapies that harness or enhance a patient's immune system to target their tumors have recently been developed (1–4). The discovery of immune checkpoint receptors, such as CTLA4 and PD-1 (5–9), that repress the activity of antitumor T cells, led to the development of blocking antibodies directed against these coinhibitory receptors or their ligands, including ipilimumab (anti-CTLA4), pembrolizumab (anti–PD-1), nivolumab (anti–PD-1), atezolizumab (anti–PD-L1), and durvalumab (anti–PD-L1). Strikingly, some patients treated with checkpoint inhibitors experience durable tumor regression, in contrast to targeted small-molecule therapies where tumor relapse is a common occurrence (10). This remarkable response has led to the rapid approval of these therapies for patients and a tremendous amount of optimism in the field (4, 10, 11).

However, despite promising clinical results, checkpoint blockade therapies are successful in only a subset of patients, and certain tumor types respond more favorably than others (11). Furthermore, it is increasingly appreciated that, as in the case of targeted therapies, tumors can acquire resistance against immunotherapies (12–14). Thus, it is crucial to more fully understand the mechanisms behind immunotherapies to develop complementary treatments that will broaden the types of tumors that respond to immunotherapy, and to further enhance the specificity and efficacy of antitumor activity of existing approaches.

One potential strategy is to pair immunotherapies with small-molecule inhibitors. There are many advantages to small-molecule drugs in comparison with antibody-based biologics, including greater exposure in the tumor microenvironment and access to intracellular targets (15). Moreover, increasing evidence indicates that signaling from oncogenic driver kinases, such as mutant BRAF in melanoma (16) or mutant EGFR in lung cancer (17), in addition to their role in promoting cellular transformation, can alter the tumor microenvironment to promote immunosuppression, and inhibition of these oncogenes using small-molecule drugs can contribute to immune reactivation. Furthermore, small-molecule

[1]Department of Medical Oncology, Dana-Farber Cancer Institute, Boston, Massachusetts. [2]Division of Hematology & Medical Oncology, Laura and Isaac Perlmutter Cancer Center, New York University Langone Medical Center, New York, New York. [3]Department of Cancer Biology, Dana-Farber Cancer Institute, Department of Biological Chemistry and Molecular Pharmacology, Harvard Medical School, Boston, Massachusetts. [4]Division of Medical Oncology, Massachusetts General Hospital Cancer Center, Harvard Medical School, Boston, Massachusetts. [5]Department of Biostatistics and Computational Biology, Dana-Farber Cancer Institute, Boston, Massachusetts. [6]Department of Pediatric Oncology, Dana-Farber Cancer Institute, Boston, Massachusetts. [7]Belfer Center for Applied Cancer Science, Dana-Farber Cancer Institute, Boston, Massachusetts. [8]Center for Molecular Oncologic Pathology, Dana-Farber Cancer Institute, Boston, Massachusetts. [9]G1 Therapeutics, Research Triangle Park, North Carolina. [10]Division of Thoracic Surgery, Brigham and Women's Hospital, Boston, Massachusetts. [11]Department of Surgery, Massachusetts General Hospital, Harvard Medical School, Boston, Massachusetts. [12]Department of Medicine, Brigham and Women's Hospital, Harvard Medical School, Boston, Massachusetts. [13]Division of Hematologic Malignancies, Dana-Farber Cancer Institute, Boston, Massachusetts. [14]The Lineberger Comprehensive Cancer Center, University of North Carolina School of Medicine, Chapel Hill, North Carolina.

Note: Supplementary data for this article are available at Cancer Discovery Online (http://cancerdiscovery.aacrjournals.org/).

J. Deng, E.S. Wang, and R.W. Jenkins contributed equally to this article.

Corresponding Authors: Kwok-Kin Wong, New York University Langone Medical Center, 550 1st Avenue, Smilow 1011, New York, NY 10016. Phone: 212-263-9203; Fax: 617-632-7839; E-mail: kwok-kin.wong@nyumc.org; Nathanael S. Gray, DFCI Department of Cancer Biology, Longwood Center, Room 2209, 360 Longwood Avenue, Boston, MA 02215. Phone: 617-582-8590; Fax: 617-582-8615; E-mail: Nathanael_Gray@dfci.harvard.edu; and David A. Barbie, 450 Brookline Avenue, D819, Boston, MA 02215. Phone: 617-632-6049; E-mail: dbarbie@partners.org

doi: 10.1158/2159-8290.CD-17-0915

inhibitors can directly alter immune cell function and contribute to antitumor immunity, as was reported in a recent study where inhibition of MAPK kinase (MEK) increased levels of effector $CD8^+$ T cells in tumors and synergized with anti–PD-L1 blockade (18). As such, combining small-molecule kinase inhibitors, which induce dramatic but short-lived tumor regression, with immunotherapies, which have slower but potentially more durable responses, is an attractive potential treatment strategy that can be applied to different cancer types with distinct oncogenic driver genes.

Cyclin-dependent kinases (CDK) are a family of proline-directed serine/threonine kinases that are conserved across eukaryotes (15). The classical cell-cycle CDKs (1, 2, 4, and 6) regulate checkpoints to ensure proper progression through the cell cycle (19), and thus have long been attractive targets for pharmacologic inhibition for treating cancers. In particular, the CDK4/6 inhibitors palbociclib, ribociclib, and abemaciclib recently received FDA approval for the treatment of patients with advanced or metastatic breast cancers, and are in clinical trials for other indications, including non–small cell lung cancer. Although best known for their function in phosphorylating retinoblastoma (Rb) to promote cell-cycle progression, there is increasing evidence that CDK4/6 regulate lymphocytes in other ways (19). For example, CDK6 was recently reported to control hematopoietic stem cell activation via transcriptional repression of the transcription factor EGR1 (20, 21).

In this study, we identified a role for CDK4/6 in modulating T-cell activation via regulation of the activity of NFAT proteins, a family of transcription factors crucial for T-cell activation (22). Furthermore, we found that pharmacologic inhibition of CDK4/6 increased levels of tumor-infiltrating T cells *in vivo*, and synergized with anti–PD-1 blocking antibodies in multiple syngeneic tumor models. Taken together, our results uncover a mode of action for CDK4/6 inhibitors and suggest that treatment with CDK4/6 inhibitors may increase the effectiveness of immune checkpoint blockade therapies in patients.

RESULTS

Small-Molecule Screen Identifies CDK4/6 Inhibitors as Compounds that Enhance T-cell Activity

To identify small molecules capable of enhancing T-cell activation in the setting of PD-1 engagement, we screened for compounds that activate PD-1–overexpressing Jurkat T cells (23) by measuring IL2 secretion following α-CD3/CD28/IgG ("TCR/IgG") or α-CD3/CD28/PD-1 ("TCR/PD-1") stimulation (Fig. 1A; Supplementary Fig. S1A). In addition to known negative regulators of IL2 production [e.g., glycogen synthase kinase-3α/β (GSK3α/β); refs. 24, 25], this screen identified cyclin-dependent kinase 4 and 6 inhibitors (CDK4/6i) as top hits (Supplementary Table S1). As immunostimulatory properties have not been previously ascribed to CDK4/6i, we tested several optimized inhibitors, including the three FDA-approved compounds palbociclib, ribociclib, and abemaciclib, as well as trilaciclib (G1T28), a recently reported selective CDK4/6 inhibitor (26, 27), and found that three of the four tested compounds potently enhanced IL2 secretion, even when suppressed by PD-1 signaling (Fig. 1B). Although abemaciclib had the greatest stimulatory activity, kinome profiling revealed that it potently inhibits many other kinases, including GSK3α/β (Supplementary Fig. S1B–S1D and published data; ref. 26). As palbociclib and trilaciclib are significantly more selective for CDK4/6, we sought to minimize potential confounding effects due to off-target activity and focused our studies on these two compounds.

To further investigate this phenomenon, we stimulated primary human $CD4^+$ T cells with α-CD3/CD28 and either recombinant PD-L1 or control IgG, and found that both palbociclib and trilaciclib treatment enhanced IL2 secretion (Fig. 1C). This recapitulated the effect we observed in Jurkat cells, confirming that CDK4/6i have potent immunostimulatory activity. Importantly, transfection of CDK4- or CDK6-specific siRNAs (Fig. 1D) revealed that knockdown of CDK6, but not CDK4, enhanced IL2 secretion (Fig. 1E), supporting on-target specificity of small-molecule CDK4/6 inhibitors and a predominant role for CDK6 inhibition.

To verify this discovery in a more physiologic setting, patient-derived organotypic tumor spheroids (PDOTS) were treated with CDK4/6i (Supplementary Fig. S1E) in a novel *ex vivo* three-dimensional (3-D) microfluidic culture system (28). PDOTS contain autologous tumor-infiltrating immune cells (Supplementary Fig. S1F and S1G), and bead-based cytokine profiling of conditioned media from spheroids loaded into 3-D microfluidic devices revealed increased levels of TH1 cytokines (e.g., CXCL9, CXCL10, IFNγ, IL16, and CXCL16; refs. 29, 30) following treatment with palbociclib or trilaciclib (Fig. 1F and G). Although the concentration of IL2 was below the detection range in this system, these findings suggest that CDK4/6i may activate CTL/TH1 responses to elicit antitumor immunity.

CDK6 Regulates NFAT Activity

NFAT family proteins are crucial for T-cell activation and transcriptional regulation of *IL2* (22). To investigate the link between CDK4/6 and NFAT in regulating IL2 production, we measured IL2 secretion from PD-1–overexpressing Jurkat cells stimulated in the presence of palbociclib and cyclosporine A (CsA), a calcineurin inhibitor that prevents activation of the NFAT pathway (Fig. 2A). Addition of CsA ablated the production of IL2, even in the presence of palbociclib, suggesting that CDK4/6 inhibitors increase IL2 secretion through heightened NFAT signaling and not via an alternative pathway. Interestingly, a recent biochemical screen suggested that NFAT4 (*NFATc3*) is a substrate of CDK4/6 (31). To assess phosphorylation of NFAT4 by CDK4/6, we performed two-dimensional (2-D) ^{15}N heteronuclear single quantum correlation (2-D–HSQC) experiments to analyze changes in chemical shifts of the regulatory domain of NFAT4 after incubation with either recombinant CDK4/Cyclin D1 or CDK6/Cyclin D3. The ^{15}N HSQC spectrum of NFATc3 (1–400) has narrow dispersion (~1 ppm) in the ^1H dimension centered on the random coil chemical shift of 8.0 ppm, consistent with an unstructured protein (Supplementary Fig. S2A). The few resonances around the ^1H frequency of 7.5 ppm indicate that a minor part of this protein harbors structured elements, which is in accordance with the disorder prediction from primary sequence information (Supplementary Fig. S2C). When NFAT4 was

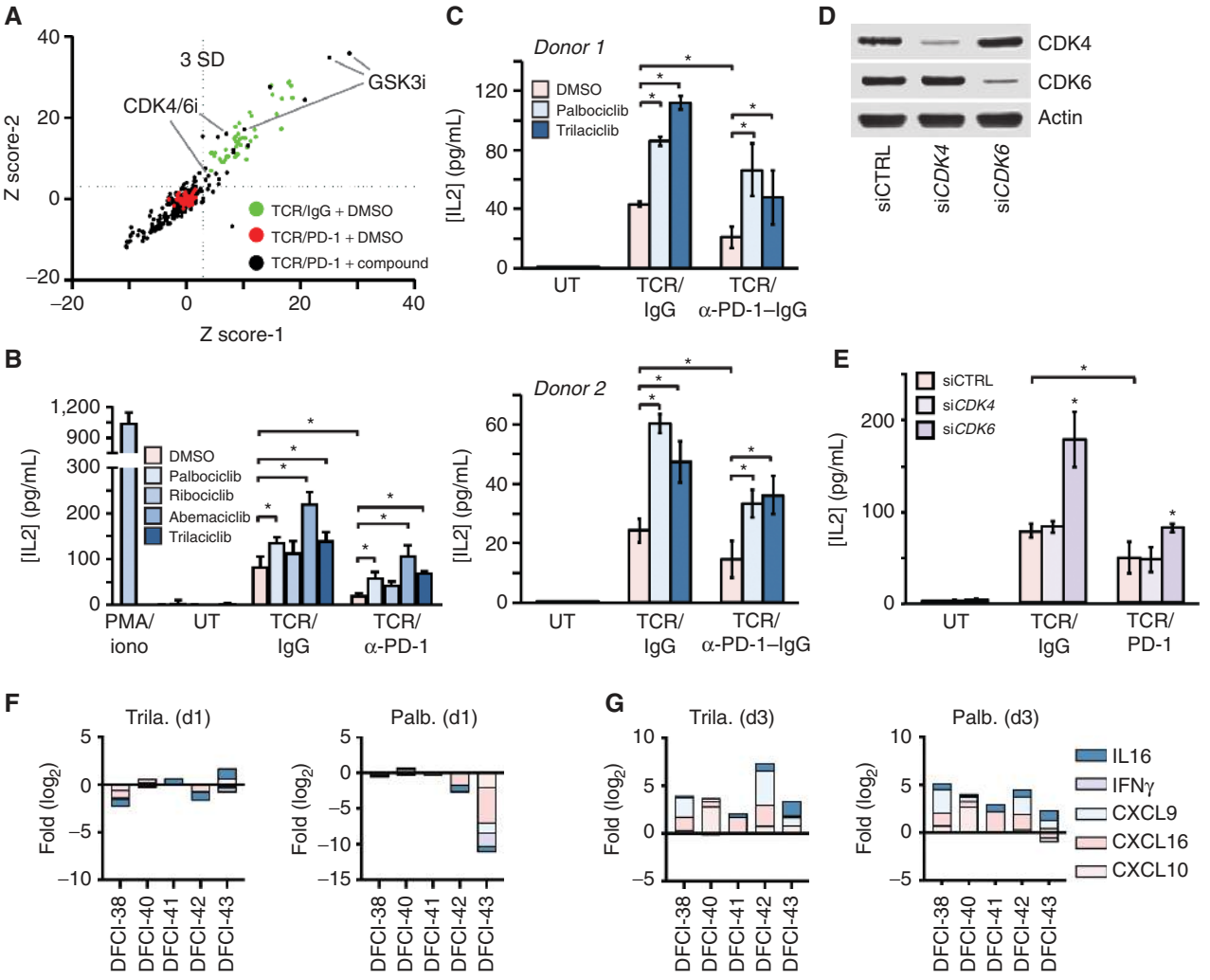

Figure 1. Small-molecule CDK4/6 inhibitors enhance IL2 secretion from T cells. **A,** Plot of replicate Z scores from the screening of small-molecule compounds capable of enhancing IL2 secretion from stimulated PD-1–Jurkat cells with compounds annotated as GSK3α/β or CDK4/6 inhibitors labeled. **B,** Quantification of IL2 levels by ELISA from PD-1–Jurkat cells treated with PMA/ionomycin or 1 μmol/L CDK4/6 inhibitors and stimulated as indicated for 18 hours. Results shown as mean ± SD [untreated (UT), $n = 2$; other conditions, $n = 5$; *, $P < 0.05$]. **C,** Quantification of IL2 levels by ELISA from primary human CD4+ T cells treated with 100 nmol/L palbociclib (Palb.) or trilaciclib (Trila.) and stimulated as indicated. Results shown as mean ± SD (UT, $n = 2$; other conditions, $n = 4$; *, $P < 0.05$). **D,** Immunoblot for CDK4 and CDK6 from PD-1–Jurkat cells transiently transfected with the indicated siRNA. **E,** Quantification of IL2 levels from PD-1–Jurkat cells after transient transfection with siRNA against *Cdk4* or *Cdk6* and stimulated as indicated for 18 hours. Results shown as mean ± SD ($n = 4$; *, $P < 0.05$). Cytokine profiling analysis from human patients using patient-derived organotypic tumor spheroids (PDOTS) cultured in a 3-D culturing system at day 1 (**F**) and day 3 (**G**). Freshly obtained patient samples were digested into spheroids and treated with indicated drugs in the 3-D microfluidic system. Cytokine secretion was analyzed by Luminex and expressed as $\log_2$ fold change relative to untreated control.

incubated with CDK6, we observed the appearance of resonances corresponding to phospho-serine residues, upfield of 8.5 ppm in the ^{1}H dimension, and a number of distinct chemical shift perturbations for the residues neighboring the phosphorylation sites (Supplementary Fig. S2A; refs. 32, 33). However, this did not occur when NFAT4 was incubated with CDK4 (Supplementary Fig. S2A), consistent with our previous knockdown data (Fig. 1D and E), although we observed some nonspecific peak broadening due to the presence of glycerol in the enzyme mixture. Importantly, CDK6-induced phosphorylation of NFAT4 was inhibited when the kinase was preincubated with palbociclib (Supplementary Fig. S2B), where we observed neither phospho-serine resonances nor distinct chemical shift perturbations associated with phosphorylation. Although we observed the broadening of a few resonances after the addition of palbociclib, we confirmed that this was a nonspecific effect due to the addition of DMSO (Supplementary Fig. S2B).

As our nuclear magnetic resonance (NMR) results indicated that CDK6 is an upstream NFAT kinase, we hypothesized that CDK4/6i would result in decreased phospho-NFAT, which could lead to increased nuclear translocation and enhanced NFAT transcriptional activity (22, 26). As we were unable to assign the residues of NFAT4 that were phosphorylated

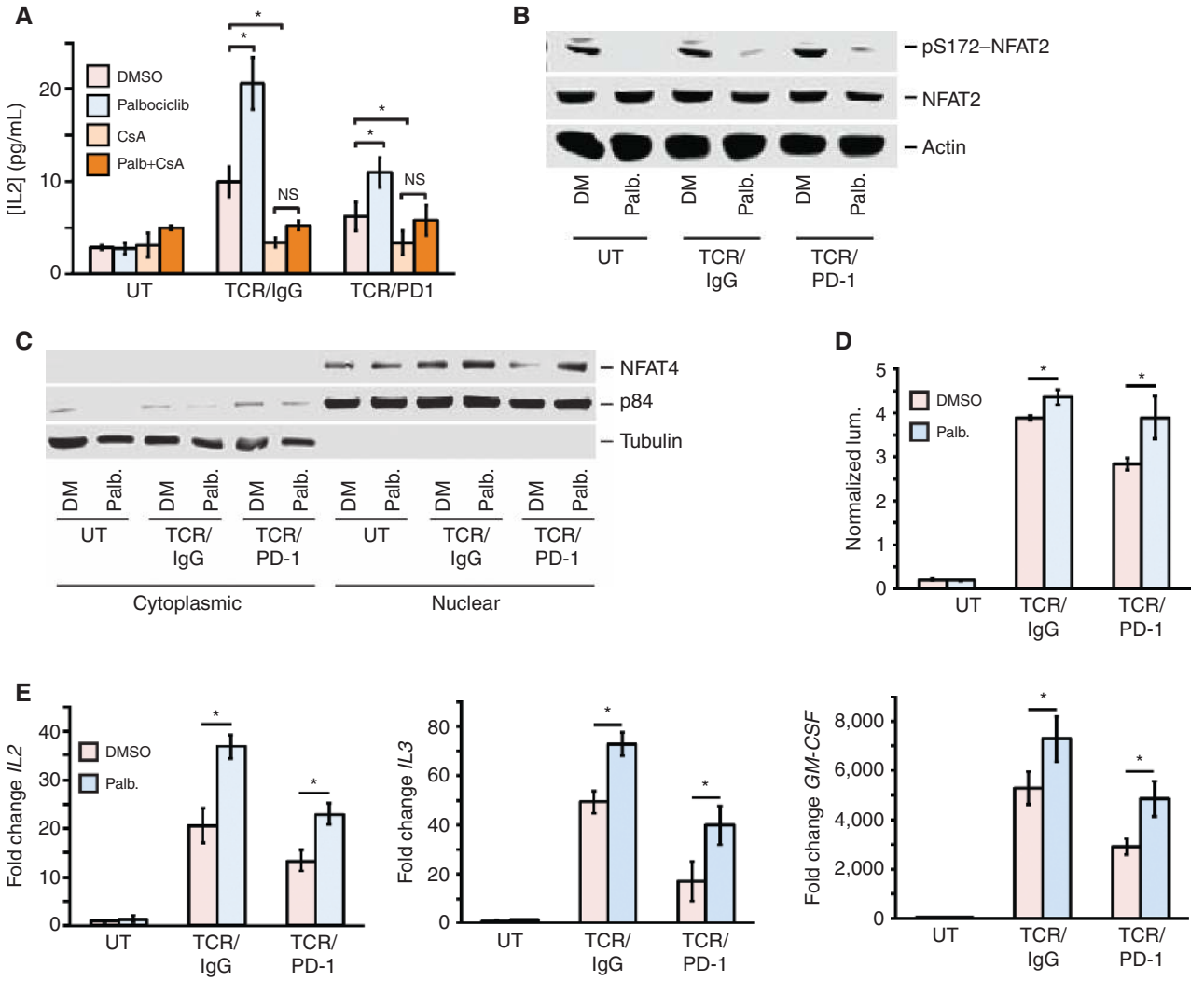

Figure 2. CDK4/6 inhibition derepresses NFAT activity. **A,** Quantification of IL2 levels from PD-1–Jurkat cells treated with 1 μmol/L palbociclib (Palb.) and/or 1 μmol/L cyclosporine A (CsA) and stimulated as indicated for 18 hours. Results shown as mean ± SD (UT, $n = 2$; other conditions, $n = 4$; *, $P < 0.05$). **B,** Immunoblot for levels of phospho-S172 and total NFAT2 after treatment of PD-1–Jurkat cells with 1 μmol/L palbociclib and stimulated as indicated for 18 hours. **C,** Immunoblot for NFAT4 from nuclear and cytoplasmic fractions of PD-1–Jurkat cells treated with 1 μmol/L palbociclib and stimulated as indicated for 18 hours. **D,** Normalized luminescence of PD-1–Jurkat cells transiently transfected with NFAT-FLuc and RLuc-SV40 reporters after treatment with 1 μmol/L palbociclib and stimulated as indicated for 18 hours. Results shown as mean ± SD ($n = 3$; *, $P < 0.05$). **E,** Relative levels of *IL2, IL3,* and *GM-CSF* mRNA as measured by qPCR from PD-1–Jurkat cells treated with 1 μmol/L palbociclib and stimulated as indicated for 8 hours. Results shown as mean ± SD ($n = 3$; *, $P < 0.05$ by two-way ANOVA with Bonferroni correction for multiple comparisons).

by CDK6, we instead examined levels of phospho-Ser172-NFAT2, a site reported to regulate the nuclear localization of NFAT2 (34). Although we do not have evidence that CDK4/6 directly phosphorylates NFAT2, we found that treatment of PD-1–Jurkat cells with palbociclib reduced levels of phospho-Ser172-NFAT2 (Fig. 2B), suggesting that multiple members of the NFAT family may be regulated by CDK4/6.

As phosphorylation of the regulatory domains of NFATs is a key regulator of their nuclear localization, we isolated nuclear and cytoplasmic fractions from unstimulated or stimulated PD-1–Jurkat cells treated with palbociclib or vehicle control, and found that CDK4/6 inhibition increased nuclear levels of NFAT4 (Fig. 2C). Consistent with increased levels of NFATs in the nucleus, we also found that exposure to palbociclib increased NFAT transcriptional activity (Fig. 2D) and mRNA expression of *IL2, IL3*, and *GM-CSF* (Fig. 2E), three previously reported NFAT targets (35). Taken together, these results reveal a novel role for CDK6 as an upstream regulator of NFAT activity, and demonstrate that pharmacologic CDK4/6 inhibition can enhance T-cell activation *in vitro*.

CDK4/6 Inhibition Enhances T-cell Infiltration into Lung Tumors

To determine the impact of CDK4/6 inhibition on tumor-infiltrating immune cells *in vivo*, we treated $Kras^{LSL\text{-}G12D}Trp53^{fl/fl}$

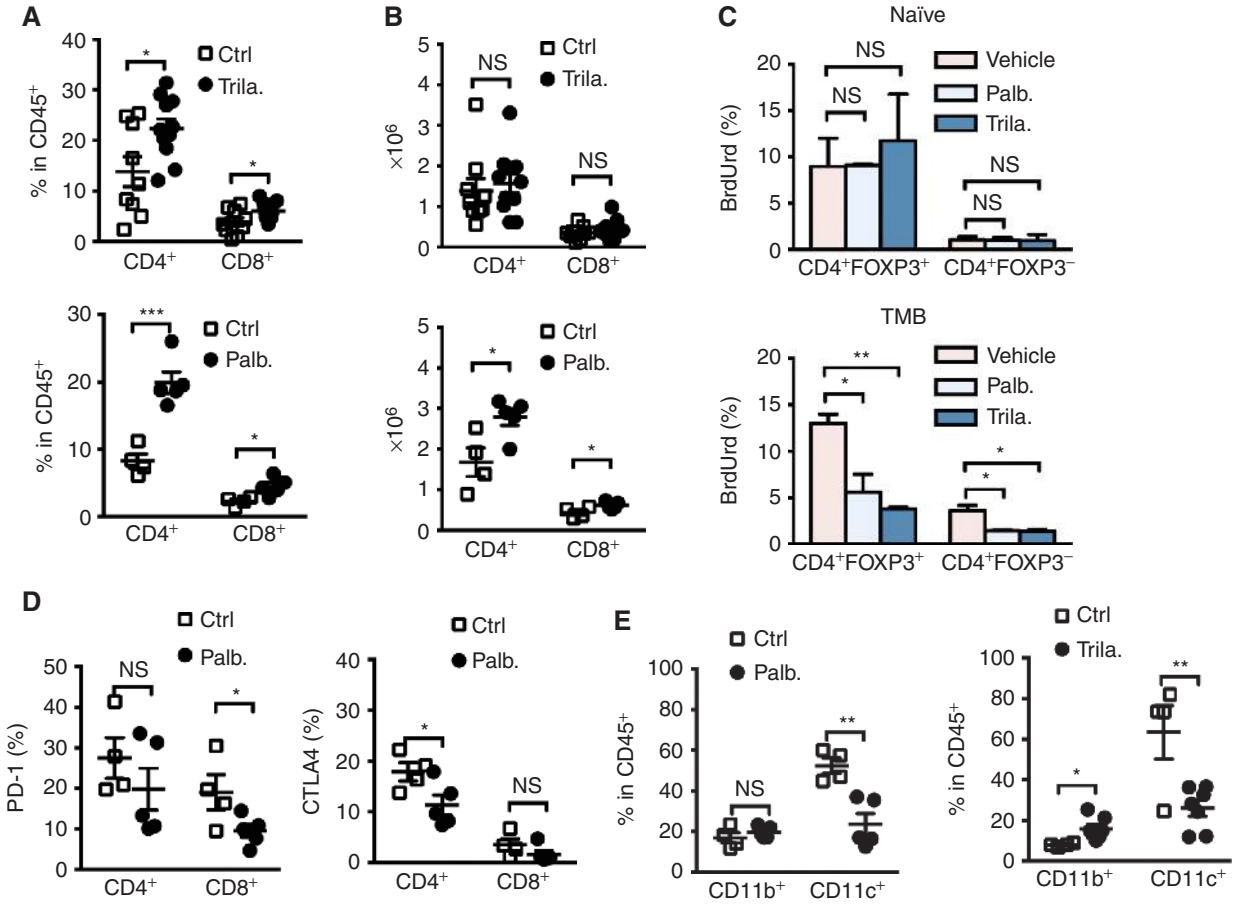

Figure 3. Analysis of immune infiltrates of lung tumor after CDK4/6 inhibition. Genetically engineered mouse model (GEMM) harboring the *Kras*$^{LSL\text{-}G12D}$*Trp53*$^{fl/fl}$ mutation was induced by Ad-Cre recombinase for lung tumors. After verification of tumor formation by MRI scan, mice were then treated with either trilaciclib (Trila.) or palbociclib (Palb.) every day for 7 days, after which lung tissues were collected for FACS analysis. Results shown are pooled from three independent experiments. Lung infiltrating T cells percentage among total CD45$^+$ leukocytes (**A**) or absolute cell number (**B**) after treatment with trilaciclib ($n = 8$) or palbociclib (ctrl, $n = 4$, Palb., $n = 5$; *, $P < 0.05$; ***, $P < 0.001$). **C,** BrdUrd incorporation by T cells shows proliferation affected by CDK4/6 inhibitors trilaciclib or palbociclib. Mice without (naïve, top) or with (TMB, bottom) *Kras*$^{LSL\text{-}G12D}$*Trp53*$^{fl/fl}$ (KP) allograft tumors were treated with trilaciclib or palbociclib, followed by systemic BrdUrd injection (i.p.). BrdUrd incorporation within different T-cell subpopulations Treg (CD4$^+$FOXP3$^+$) and Tconv (CD4$^+$FOXP3$^-$) was determined by flow cytometry ($n = 6$; *, $P < 0.05$; **, $P < 0.01$). **D,** Expression levels of PD-1 and CTLA4 in CD4$^+$ or CD8$^+$ T cells infiltrated at tumor site after treatment (ctrl, $n = 4$, Palb., $n = 5$; *, $P < 0.05$). **E,** Changes in levels of CD11b$^+$ and CD11c$^+$ myeloid subpopulations after trilaciclib ($n = 8$) or palbociclib (ctrl, $n = 4$, Palb., $n = 5$) treatment (*, $P < 0.05$; **, $P < 0.01$).

(KP) mice, representing an immunocompetent genetically engineered mouse model (GEMM) of human non–small cell lung cancer (36), with either palbociclib or trilaciclib. Both agents increased infiltration of CD4$^+$ T cells and CD8$^+$ cells, to a lesser degree, into lung tumors among total lung-infiltrating leukocytes (Fig. 3A). This increase of CD4$^+$ cells was confirmed in two additional GEMMs, including the *Kras*$^{LSL\text{-}G12D}$ (K) and the *Kras*$^{LSL\text{-}G12D}$*Lkb1*$^{fl/fl}$ (KL) model (36), in which CDK4/6i also increased infiltration of tumor-infiltrating leukocytes (TIL) into lung tumors (Supplementary Fig. S3A).

Although CDK6 plays a critical role in T-cell proliferation (26, 37), transient inhibition of CDK4/6 did not decrease total number of TILs in these lung tumors, whereas absolute numbers of CD4$^+$ and CD8$^+$ cells only mildly changed (Fig. 3B). This finding suggests that CDK4/6 inhibition can either induce intratumoral T-cell expansion, which is unlikely given the requirement for CDK4/6 for cell proliferation (19), or can lead to increased homing of effector T cells to the tumor. To explore the impact of CDK4/6i on TIL proliferation, we evaluated bromodeoxyuridine (BrdUrd) incorporation *in vivo*. CDK4/6i did not alter BrdUrd incorporation in CD4$^+$ or CD8$^+$ cells from naïve mice without tumors (Fig. 3C, top; Supplementary Fig. S4A), but did diminish BrdUrd incorporation in both CD4$^+$FOXP3$^-$ conventional T cells (Tconv) and CD4$^+$FOXP3$^+$ regulatory T cells (Treg), but not CD8$^+$ cells, isolated from mice bearing *Kras*$^{LSL\text{-}G12D}$*Trp53*$^{fl/fl}$ allografts (Fig. 3C, bottom, Supplementary Fig. S4A). Similarly, CDK4/6i more potently reduced proliferation of T cells from tumor-bearing mice than naïve mice after stimulation *ex vivo* (Supplementary Fig. S4A and S4B), possibly because proliferation of naïve T cells relies on CDK1 and other transcriptional factors such as T-bet (19, 38), whereas tumor-infiltrating CD4$^+$ lymphocytes are more susceptible to CDK4/6i. However, the percentage of Tregs did not show significant changes among

$CD4^+$ TILs after CDK4/6i treatment (Supplementary Fig. S3B and S3C).

We next evaluated the impact of CDK4/6i on the immune microenvironment beyond T-cell proliferation and IL2 secretion by investigating chemokines, expression of exhaustion markers, and the proliferation of other stromal cells. Levels of the Th1 chemokines CXCL9 and CXCL10, which govern the trafficking of effector T cells to tumor sites (30, 39), were increased in the lung after CDK4/6 inhibition (Supplementary Fig. S4C and S4D). Levels of coinhibitory molecules, including PD-1 and CTLA4, were reduced in both $CD4^+$ and $CD8^+$ T cells after palbociclib or trilaciclib treatment, albeit to different extents (Fig. 3D; Supplementary Fig. S3D and S3E). CDK4/6i also reduced the abundance of $CD11c^+$ myeloid cells (Fig. 3E), which may be due to decreased proliferation of bone marrow hematopoietic progenitors (26). We also observed reduced levels of IL6, IL10, and IL23 after CDK4/6i (Supplementary Fig. S4D), three cytokines produced by myeloid cells that suppress the TH1 response in cancer (40, 41). Taken together, these data indicate that despite effects on T-cell proliferation, CDK4/6 inhibition results in an increased percentage of effector cells within the tumor microenvironment, correlated to chemokine secretion, with apparent downregulation of coinhibitory molecules in some of the models tested. Moreover, the antiproliferative effect of CDK4/6i does not result in an increase of Tregs among TILs, but does result in a reduced number of the myeloid subpopulation.

Tumor Antigen–Experienced T Cells More Sensitive to CDK4/6 Inhibition than Naïve T Cells

As a recent report demonstrated that lymphocyte proliferation inhibition by CDK4/6i is transient and reversible (27), it is possible that properly timed and sequenced doses of CDK4/6i can activate effector T cells without adversely suppressing their proliferation. To evaluate the impact of CDK4/6i on T-cell activation, IFNγ secretion was evaluated. Total splenocytes isolated from tumor-bearing mice, but not naïve mice, treated with trilaciclib *in vivo* demonstrated increased IFNγ secretion (Supplementary Fig. S5A and S5B). This finding was further confirmed by treatment with trilaciclib *ex vivo*, which increased IL2 production only in cells from tumor-bearing mice (Fig. 4A; Supplementary Fig. S5C). Moreover, although CDK4/6i did not significantly alter IFNγ secretion by $CD8^+$ cytotoxic T cells alone (Supplementary Fig. S5D and S5E), coculture of splenic $CD8^+$ T cells from tumor-bearing mice with Tregs in the presence of trilaciclib relieved Treg-mediated suppression, as IFNγ production increased by approximately 10-fold. In contrast, the effect of CDK4/6i on IFNγ production from naïve $CD8^+$ T cells cocultured with Tregs was minimal (Fig. 4B; Supplementary Fig. S5F). These data suggest that CDK4/6i can augment effector T-cell function even in the presence of Tregs.

To further investigate the effects of CDK4/6 inhibition on tumor-infiltrating T cells *in vivo*, we performed single-cell RNA sequencing (RNA-seq) on $CD3^+$ T cells isolated from KP GEMM lung tumors. Gene ontology (GO) analysis revealed enrichment for processes related to lymphocyte activation and proliferation (Supplementary Table S2). Several reported NFAT targets were upregulated by trilaciclib, including *Ccr2, Clcf1, Cx3cr1*, and *Cd86* (Fig. 4C; Supplementary Table S3), consistent with our *in vitro* findings (Fig. 2). Conversely, we observed downregulation of *Ccna2* and *Cd22*, which are negatively regulated by NFATs (Fig. 4C; Supplementary Table S3). Thus, single-cell RNA-seq data was consistent with our *in vitro* findings, indicating that inhibition of CDK4/6 derepresses NFAT activity.

We further analyzed the T-cell RNA-seq data by unsupervised density-based clustering on t-Distributed Stochastic Neighbor Embedding (t-SNE) analysis to separate cells into three different groups (clusters) according to gene expression signatures (Fig. 4D). One group was comprised almost exclusively of cells from trilaciclib-treated mice (group 3). A second group contained cells predominantly from trilaciclib-treated mice, but also from vehicle-treated animals (group 1). The final group (group 2) represented a mixture of cells from vehicle and trilaciclib-treated mice (Fig. 4D). Trilaciclib treatment significantly increased IL2 signaling activation in group 3, as well as in group 1, to a lesser extent. This activation includes upregulation of the IL2 receptors IL2Rα, IL2Rβ, and IL2Rγ (Fig. 4E). Treatment with trilaciclib increased the proportion of T cells in the G_1 phase in groups 1 and 3 (Supplementary Fig. S6A), confirming on-target pharmacodynamic effects in these cells. Compared with cells in group 2, cells from groups 1 and 3 showed evidence of highly activated NFAT signaling (Supplementary Fig. S6E), along with heightened upregulation of activation markers, including *4-1BB* (*Tnfrsf9*), *Icosl, GITR* (*Tnfrsf18*), *Cd40*, and *Cd86* (Fig. 4E; Supplementary Fig. S7A). Compared with group 1, cells in group 3 showed greater downregulation of inhibitory markers (42), including *Pd-l1* (*Cd274*), *Pd-l2* (*Pdcd1lg2*), *Tim3* (*Havcr2*), and *Cd200* and its receptors (Fig. 4E; Supplementary Fig. S7B). In addition, these cells demonstrated greater TCR signaling, manifested by upregulation of *Zap70, Lat, Skap1*, and *Cd6*, which are important for continued T-cell activation after

Figure 4. Tumor antigen–experienced T cells exhibit greater sensitivity to CDK4/6 inhibition. **A,** IL2 production from Tconv cells after trilaciclib treatment. $CD4^+CD25^-$ Tconv cells were isolated from either naïve or tumor-bearing (TMB) mice and treated with trilaciclib at indicated concentrations, in the presence of CD3 and CD28 stimulation. IL2 production was determined 3 days after the treatment and normalized with untreated control ($n = 3$; *, $P < 0.05$). **B,** Increased IFNγ production in $CD8^+$ T cells by trilaciclib treatment, in the presence of Treg. $CD8^+$ T cells from naïve or TMB mice were isolated and cocultured with $CD4^+CD25^+$ Treg cells (5:1 ratio), in the presence of different concentrations of trilaciclib as indicated. IFNγ production was determined 3 days after the treatment and normalized with untreated control ($n = 3$; *, $P < 0.05$, **, $P < 0.01$). **C,** Violin plot of expression levels of NFAT-regulated genes determined by single-cell RNA-seq of tumor-infiltrating $CD3^+$ T cells from KP GEMM mice 7 days after trilaciclib treatment. **D,** t-SNE plot showing distinct homogenous groups of T cells identified with density-based clustering (dbscan). **E,** Heat map showing transcriptional levels of genes from each cell that are important for T-cell activation and suppression, and IL2 and TCR signaling. The status of each cell including treatment status and group identification is shown below the heat map as bar graphs. Each column represents one cell.

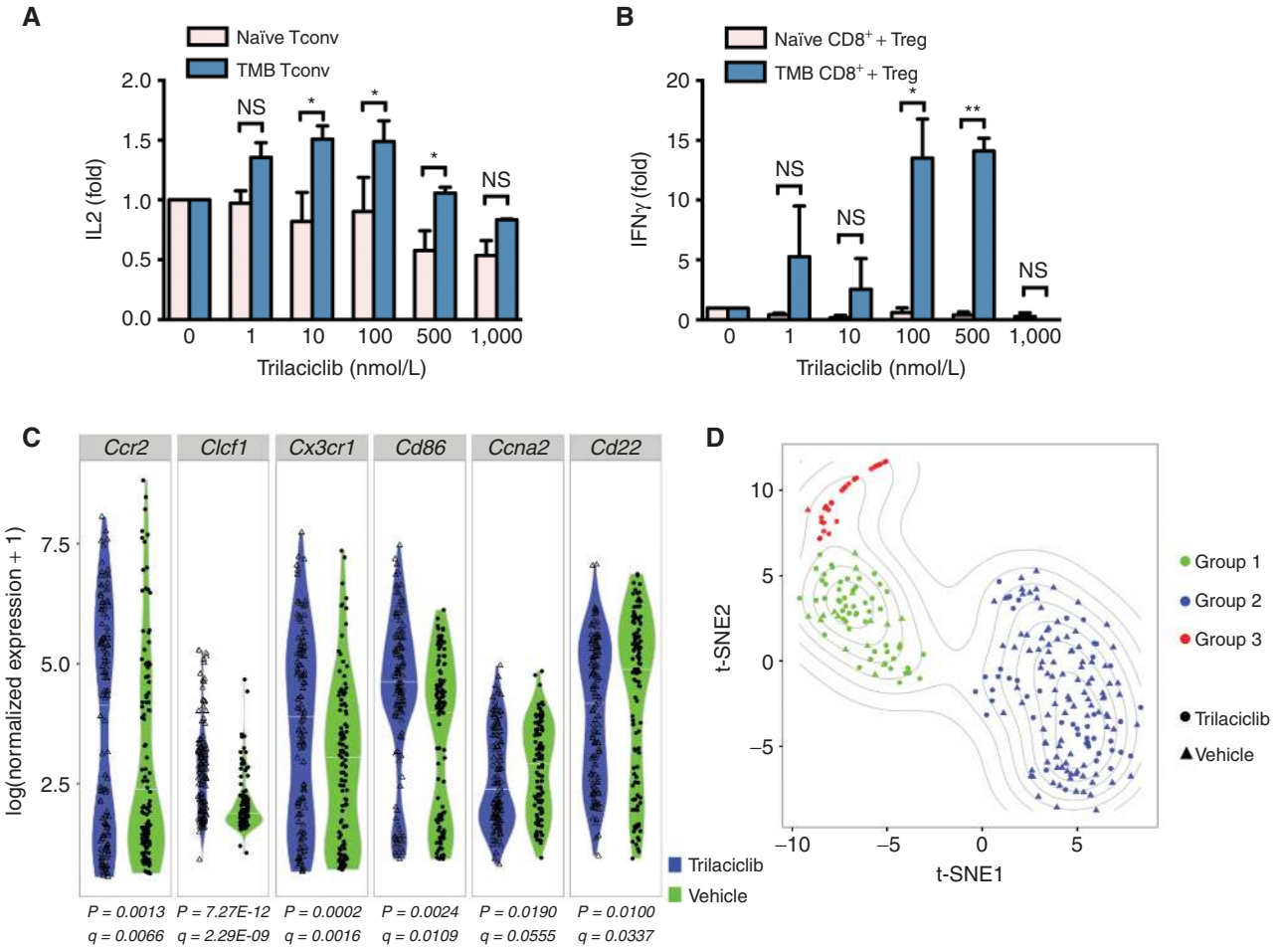

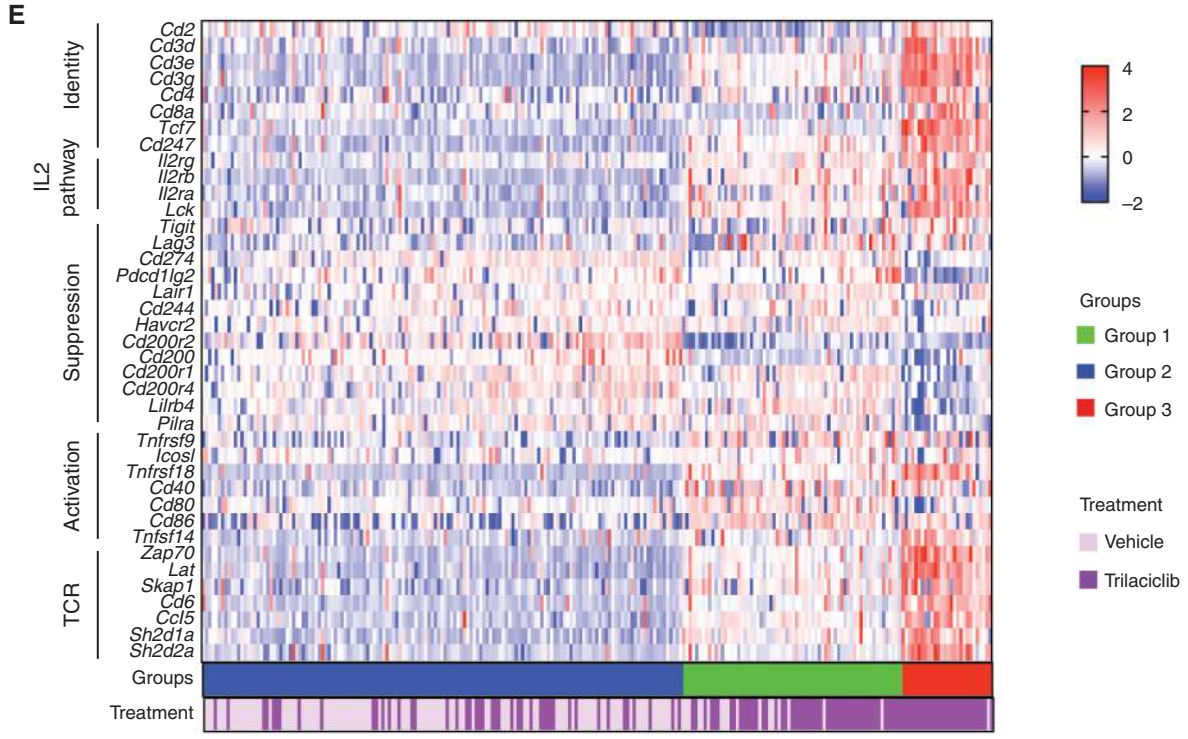

TCR engagement, as well as for the effector T-cell function (Fig. 4E). Interestingly, these hyperactive cells were primarily in the G_1 phase (Supplementary Fig. S6B), consistent with the effect of CDK4/6 inhibition on traversal from G_1–S in both cancer cells and immune cells (Supplementary Fig. S6). Therefore, despite inhibitory effects on cell-cycle progression, short-term exposure to a CDK4/6i resulted in a gene transcription signature consistent with enhanced T-cell function.

CDK4/6 Inhibition Augments Anti–PD-1 Antibody–Induced Antitumor Immunity

We next examined effects of CDK4/6i on tumor burden. CDK4/6i alone was not sufficient to eradicate tumors despite reduced tumor proliferation and increased T-cell activation and infiltration in the KP GEMM model (Fig. 5A), consistent with a previous report that palbociclib reduces the growth of *Kras*-driven murine lung tumors (43). We therefore evaluated the ability of CDK4/6i to complement PD-1 blockade. As *Kras*-mutant GEMMs are not responsive to checkpoint blockade (3, 44), in part due to the low levels of somatic mutations (45), we utilized the murine syngeneic colon adenocarcinoma model MC38. We first demonstrated that anti–PD-1 combined with CDK4/6i synergistically induced cell death *ex vivo* in MC38 murine-derived organotypic tumor spheroids (MDOTS; ref. 28; Fig. 5B; Supplementary Fig. S8A). Furthermore, combination treatment of CDK4/6i with PD-1 blockade downregulated levels of CCL2, CXCL1, and CCL3, which negatively regulate the TH1 response (Fig. 5C). However, when MDOTS were generated from tumors grown in *Rag1*$^{-/-}$ immunodeficient mice, which lack both B and T lymphocytes, or when the TH1 response was blocked by addition of an anti-IFNγ neutralizing antibody, we no longer observed synergistic effects of CDK4/6i combined with anti–PD-1 treatment (Supplementary Fig. S8B and S8C). In contrast, addition of a neutralizing antibody against CCL5 had no such rescue effect (Supplementary Fig. S8C), suggesting that the T cells are the key cellular mediators of the antitumor activity of CDK4/6i.

T Cells Are Required for Antitumor Immunity Induced by Combinational Treatment of CDK4/6 Inhibitor and Anti–PD-1 Antibody

As previously reported, *in vivo* PD-1 blockade induced partial tumor growth inhibition in the MC38 model (46); however, consistent with the results in MDOTS, the addition of intermittent exposure to trilaciclib nearly eliminated tumor growth (Fig. 6A, left). Furthermore, we found that treatment with palbociclib in combination with PD-1 blockade had a similar effect in mice bearing tumors derived from CT26 colon carcinoma cells (47), which are far less responsive to PD-1 blockade alone (Fig. 6A, right; Fig. 6B).

Profiling of TILs from MC38 tumors revealed that anti–PD-1 alone increased CD8$^+$ IFNγ production but not CD4$^+$ IL2 production (Fig. 6C). Thus, in this model, PD-1 blockade increased the cytotoxicity of CD8$^+$ T cells, but did not increase T-cell proliferation through IL2. Addition of trilaciclib to PD-1 blockade resulted in an approximately 10-fold increase in the levels of IFNγ in CD8$^+$ TILs and approximately 2-fold increase in CD4$^+$ IL2 production (Fig. 6C). The increase in IL2 was also observed in the CT26 model treated with palbociclib alone or in combination with PD-1 (Supplementary Fig. S9A). Of note, in the MC38 model, IL2 production was also increased in the murine inguinal lymph nodes (Supplementary Fig. S9B), albeit to a lesser extent, compared with TILs, whereas IFNγ levels remained unchanged (Fig. 6D).

Importantly, we found that depletion of either CD4$^+$ or CD8$^+$ T cells in the CT26 model reversed the antitumor effect induced by combined treatment of palbociclib and anti–PD-1 (Fig. 6E). As T-cell depletion completely ablated the antitumor activity of the combination treatment, the predominant antitumor activity of palbociclib in this model could not be independent of T cells (i.e., a direct antiproliferative effect on tumor cells due to tumor cell CDK4/6 inhibition); instead, our results demonstrate that palbociclib amplifies the T cell–dependent antitumor effects of PD-1 blockade. Finally, combination treatment of CDK4/6i and PD-1 blockade was superior to single agents alone in treating established tumors, although eventual relapse was evident in all treatment groups (Supplementary Fig. S9C and S9D). Thus, CDK4/6 inhibitors greatly potentiate the effects of PD-1 blockade *in vivo*, and the major factors of the CDK4/6i-induced antitumor immune response are T cells.

DISCUSSION

Here, we show that pharmacologic inhibition of CDK4/6 promotes T-cell activation. Beginning with an unbiased small-molecule screen, we identified CDK4/6 inhibitors as a class of compounds that could enhance the production of IL2, a surrogate marker for T-cell activation, even when suppressive signaling from PD-1 was enforced. Mechanistically, we identified that CDK4/6 regulated the activity of NFAT family transcription factors, which are critically important for proper activation and function of T cells. Finally, *ex vivo* and *in vivo* studies revealed that small molecule–mediated inhibition of CDK4/6 resulted in increased antitumor activity, particularly in conjunction with PD-1 blockade, and this effect was largely dependent on T cells.

Figure 5. CDK4/6 inhibitor elicits antitumor immunity and enhance cell death induced by anti-PD-1 antibody *ex vivo*. **A,** Quantification of tumor volume changes by MRI scan after treatment with trilaciclib (Trila.). Left, waterfall plot shows tumor volume response to the treatment. Each column represents one mouse. Right, representative MRI scan images (one of 24 scanned images of each mouse) show mice lung tumors before and after the treatment. Circled areas, heart. **B,** Live (AO = green)/dead (PI = red) analysis of murine-derived organotypic tumor spheroid (MDOTS) cultured in 3-D microfluidic culture at day 0, 3, and 6 following treatment of CDK4/6 inhibitors trilaciclib or palbociclib (100 nmol/L) alone or in combination with PD-1 antibody (10 μg/mL) as indicated. Top, quantification results of live/dead analysis; bottom, representative images of deconvolution fluorescence microscopy shows live/dead cells at day 6 after indicated treatment. Statistical analysis is calculated by comparing the indicated treatment group with DMSO+IgG group at day 6 (*, $P < 0.05$; **, $P < 0.01$; ***, $P < 0.001$). Scale bar, 50 μm. **C,** Cytokine secretion from MC38 MDOTS were expressed as $\log_2$-fold change (L2FC) relative to untreated control after indicated treatment.

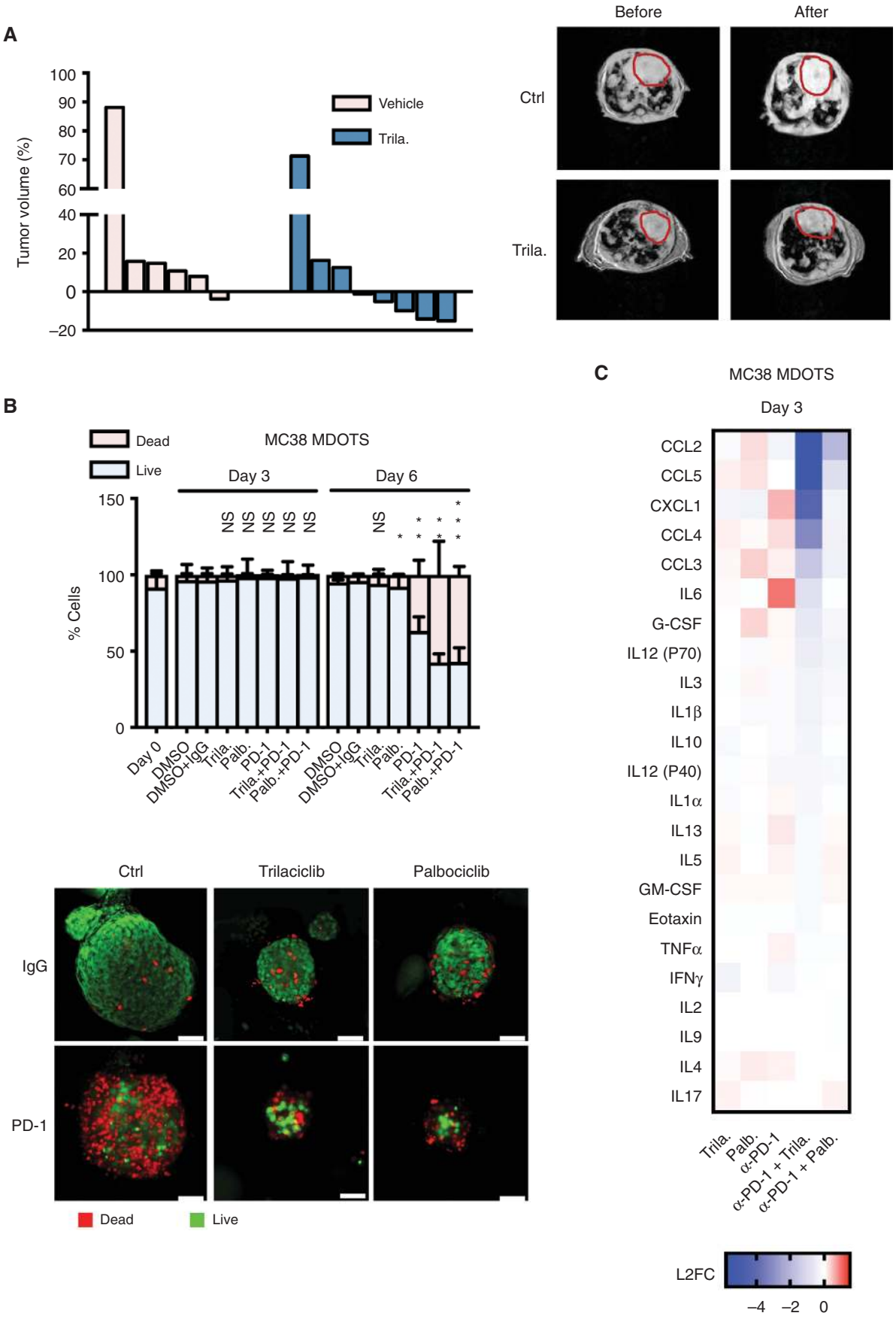

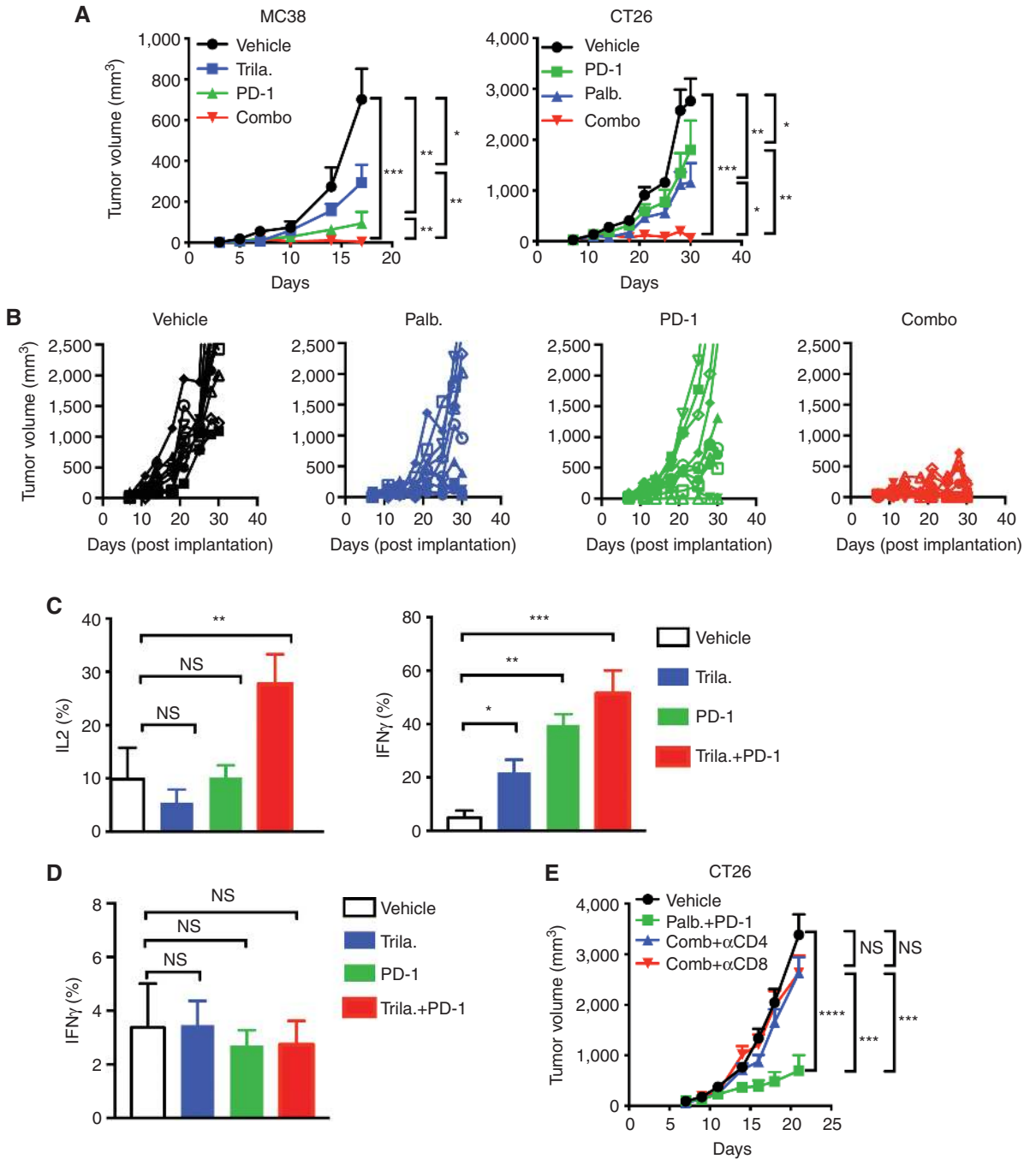

Figure 6. Combination treatment of CDK4/6 inhibitors synergize anti-PD-1 antibody–induced antitumor immunity through T cells. **A,** Tumor growth curves of MC38 (left) or CT26 (right) cells treated with CDK4/6 inhibitor or PD-1 antibody alone or in combination. MC38 murine cancer cells were injected subcutaneously into C57BL/6 mice. The mice were treated with either CDK4/6 inhibitor [trilaciclib (Trila.) or palbociclib (Palb.), 100 mg/kg] intermittently (3 days on, 4 days off) with or without PD-1 antibody (200 μg/mouse, 3 times a week) as indicated starting from day 3 (MC38) or day 7 (CT26). Tumor volumes were monitored every 2–3 days. Each graph shows representative results from two independent experiments (left, $n = 8$; right, $n = 10$; *, $P < 0.05$; **, $P < 0.01$; ***, $P < 0.001$). **B,** Individual traces of tumor volume of CT26 tumors over time after treatment with palbociclib and anti-PD-1, either alone or in combination ($n = 8$). **C,** Quantification of cytokine production produced by MC38 tumor-infiltrating T lymphocytes. At the end of the treatment (day 17), mice were sacrificed and TILs were isolated from the tumor for cytokine analysis for IL2 from $CD4^+$ T cells (left) and IFNγ from $CD8^+$ T cells (right; *, $P < 0.05$; **, $P < 0.01$; ***, $P < 0.001$). **D,** Cytokine production of IFNγ from $CD8^+$ T cells from inguinal lymph nodes of mice with MC38 tumors treated with trilaciclib at the end of treatment (day 17). **E,** Tumor growth curves of CT26 cells treated with palbociclib (100 mg/kg) and PD-1 antibody (200 μg/mouse) with or without anti-CD4 (400 μg/mouse) or anti-CD8 (400 μg/mouse) depletion antibodies. The depletion antibody treatment started at day -3 before tumor implantation was continued twice a week. Palbociclib and PD-1 were dosed at the same schedule shown in **D** starting from day 7. The graph shows representative results of two independent experiments, and the dosing and tumor measurement were performed by different people ($n = 10$; ***, $P < 0.001$; ****, $P < 0.0001$).

This finding was especially surprising because inhibiting proliferation should disrupt the clonal expansion of tumor antigen–specific T cells, thereby reducing the activity of the antitumor immune response. Instead, it is apparent that properly timed doses of CDK4/6i can promote T-cell activation and augment the effects of PD-1 blockade. Indeed, we found that short-term treatment with CDK4/6i led to heightened secretion of IFNγ from $CD8^+$ T cells in the presence of Tregs, which often correlates with enhanced antitumor cytotoxicity (3, 30). Moreover, we found in both murine models and human patient samples that treatment with CDK4/6i resulted in increased levels of TH1 cytokines/chemokines, including CXCL9 and CXCL10. As CXCL9/10 are known to be strongly induced by IFNγ, we speculate that the heightened levels of TH1 cytokines/chemokines are partly due to increased levels of IFNγ, resulting from enhanced T-cell activity after CDK4/6 inhibition.

Interestingly, our study suggests that certain types of T cells, especially T regulatory cells, are more susceptible to CDK4/6 inhibition, which may be due to differing expression levels of CDK4/6. A recent study performed transcriptional analysis of human tissue lymphocytes (including Tregs, TH1, and TH17) located either within tumors or in normal tissue (48). Interestingly, they reported that Tregs in general had higher expression of CDK6 than other T-cell subtypes, including tissue-resident TH1 and TH17 cells, as well circulating naïve, central memory, and effector memory $CD8^+$ T cells, suggesting that higher levels of CDK6 and potentially greater dependence on CDK6 in Tregs could account for their increased sensitivity to CDK4/6 inhibitors, which in turn releases suppression of IFNγ production from $CD8^+$ T cells. Future studies will be necessary to determine whether similar expression patterns occur in murine tumor models and in patients.

Although CDK4/6 are best known for their role in regulating cell-cycle progression through phosphorylation of the tumor suppressor protein RB, novel functions for these kinases have recently emerged. In particular, CDK6 has been reported to have a critical role in regulating transcription. For example, Kollmann and colleagues reported that CDK6 is a component of a transcription complex that induces the expression of the tumor suppressor $p16^{INK4a}$ (49). However, as they reported that this activity is unrelated to its kinase activity, it seems unlikely that the same mechanism is in effect in our system. In addition, Handschick and colleagues reported that CDK6 is a chromatin-bound cofactor for NFκB-dependent gene expression (50). However, they had previously found that CDK6 phosphorylates Ser536 of p65 (51), but we found that, in the setting of Jurkat cells stimulated with anti-CD3/CD28, with or without treatment with palbociclib, levels of phospho-Ser536-p65 do not change (Supplementary Fig. S10). Thus, we again do not believe that this plays a significant role in our system. Nevertheless, there is accumulating evidence that CDK6 has a critical role in regulating transcription, potentially in both kinase-dependent and kinase-independent fashions. Future studies will be necessary to carefully interrogate the transcriptional functions of CDK6 and its interacting proteins during T-cell activation.

Here, we identified that NFAT4 is a novel substrate of CDK6, but not CDK4, and that CDK4/6 inhibitors enhance NFAT activity in activated T cells. Further studies will be necessary to elucidate which other NFAT family members are direct substrates of CDK4/6, and whether NFAT activity fluctuates as cells progress through the cell cycle. Moreover, recent studies have identified NFAT signaling, in particular NFAT1 in the absence of AP1, as contributors to T-cell exhaustion (52). Although we did not find evidence of increased T-cell exhaustion after treatment with CDK4/6i, further experiments will be necessary to carefully determine the effects of using small molecules to transiently increase NFAT activity on T-cell exhaustion.

One of the chief challenges in the clinic is determining which types and subpopulations of patients will respond to any candidate immunotherapy treatment, either alone or in combination with other agents. Here, we tested a novel organotypic tumor spheroid system; as these tumor-derived spheroids are comprised of a complex mixture of tumor, immune, and stromal cells, they represent a more faithful representation of the actual tumor microenvironment. Importantly, we found that CDK4/6 inhibitors had similar effects in this *ex vivo* model as they did *in vivo*, suggesting that the MDOTS system could be an effective tool for determining whether small-molecule compounds or biologics, either as single agents or in combination, have antitumor activity without performing an *in vivo* experiment. As this technology matures, PDOTS could potentially be used as a predictive assay for determining optimal treatments in the clinic.

In summary, the effects of CDK4/6i on cell-cycle progression and T-cell proliferation are balanced favorably by increased T-cell recruitment and enhanced effector cell function in tumors, mediated in part by activation of NFAT family transcription factors. Despite the antiproliferative effects of CDK4/6i on T cells, the net result of short-term pharmacologic inhibition of CDK4/6 was augmentation of antitumor immunity, which translated to an improved antitumor response that was largely dependent on the activity of T cells. Whereas prolonged CDK4/6i treatment could be immunosuppressive due to adverse effects on lymphocyte proliferation, which has been observed in both murine models and in the clinic (27, 53, 54), properly timed and sequenced doses of CDK4/6i may potentiate the clinical impact of anti–PD-1/PD-L1 antibodies, thereby sensitizing tumors to immune checkpoint blockade. As palbociclib, ribociclib, and abemaciclib are FDA-approved and other agents are in clinical trials, we expect that this hypothesis will undergo rapid testing in humans.

METHODS

Small-Molecule Screen

PD-1–overexpressing Jurkat cells were plated at a concentration of 1×10^5 cells/well in a total volume of 80 μL. Compounds (100 nL each) from the Institute of Chemistry and Cell Biology (ICCB) EMD Kinase Inhibitor I collection (244 compounds total; ref. 55), consisting of three libraries sold by EMD as InhibitorSelect 96-Well Protein Kinase Inhibitor I (catalog no.: 539744, 80 compounds), InhibitorSelect 96-Well Protein Kinase Inhibitor II (catalog no.: 539745, 80

compounds), and InhibitorSelect 96-Well Protein Kinase Inhibitor III (catalog no.: 539746, 84 compounds), were transferred by stainless steel pin array from library plates to each assay plate. Dynabeads conjugated to α-CD3, α-CD28, and α-PD-1 antibodies were added in 20 μL, for a final assay volume of 100 μL, with a final compound concentration of 3.3 μmol/L and an 8:1 bead:cell ratio. Beads were conjugated to α-CD3/α-CD28/control IgG and added to wells containing DMSO-treated cells as a positive control, whereas beads conjugated to α-CD3/α-CD28/α-PD1 were added to wells containing DMSO-treated cells as a negative control. Supernatants from each well were analyzed for IL2 levels by AlphaLISA (PerkinElmer) according to the manufacturer's protocol. Average and SD values were calculated from the PD-1 controls (DMSO-treated cells stimulated with α-CD3/α-CD28/α-PD-1 beads); hits were defined as compounds scoring at least 3 SDs from the mean of the controls.

IL2 ELISA

PD-1–overexpressing Jurkat cells as published previously (23) were stimulated with Dynabeads conjugated to α-CD3 (UCHT1), α-CD28 (28.2), and α-PD-1 (clone EH12 from Gordon J. Freeman) or control IgG at a 4:1 bead:cell ratio in the presence of 1 μmol/L CDK4/6 inhibitor for 18 hours. For primary human T cells, normal donor human blood was obtained through Dana-Farber Cancer Institute (DFCI) Institutional Review Board (IRB) Protocol 04-430. Peripheral blood mononuclear cells (PBMC) were isolated using a Ficoll-Paque density gradient, and purified populations of $CD4^+$ T lymphocytes were obtained through a negative magnetic selection kit according to the manufacturer's instructions (Miltenyi Biotec). Primary human $CD4^+$ T cells were stimulated with Dynabeads conjugated to α-CD3 (UCHT1), α-CD28 (28.2), and recombinant hPD-L1-IgG fusion protein (from Gordon J. Freeman) or control IgG at a 4:1 bead:cell ratio in the presence of 1 μmol/L CDK4/6 inhibitor for 18 hours. IL2 levels in the supernatant were analyzed by AlphaLISA (PerkinElmer) according to the manufacturer's protocol.

KINOMEscan

Palbociclib and abemaciclib were profiled by DiscoveRx using KINOMEscan (55). Briefly, the two compounds were tested at the concentration of 100 nmol/L and 1,000 nmol/L, respectively. Targeted kinases were visualized using the TREE*spot* compound profile visualization tool. Z'LYTE kinase assays were conducted for GSK3α and GSK3β at Life Technologies using K_m ATP concentrations.

Expression and Purification of NFATc3 Regulatory Domain

The regulatory domain of human NFATc3 (residues 1–400) was cloned into a pET151/D-TOPO plasmid and expressed as a fusion protein with a N-terminal His-GB1 solubility tag cleavable with TEV protease. *Escherichia coli* strain BL21 (DE3) carrying the above plasmid was grown at 37°C in M9 media containing 6 g/L Na_2HPO_4, 3 g/L KH_2PO_4, 0.5 g/L NaCl, 1 mmol/L $MgSO_4$, 0.1 mmol/L $CaCl_2$ in H_2O supplemented with 4 g/L ^{12}C-glucose, and 1 g/L of $^{15}NH_4Cl$ isotopes. Protein expression was induced at an optical density of 0.7 by 1 mmol/L isopropyl β-D-1-thiogalactopyranoside (IPTG) at 20°C. Cells were grown for an additional 15 hours at 20°C before harvesting. The harvested cells were resuspended in 40 mL of 50 mmol/L Tris-HCl (pH 8.0), 350 mmol/L NaCl, 10 mmol/L imidazole, and 5 mmol/L β-mercaptoethanol (β-ME). The suspended cells were then disrupted by sonication, and the insoluble fraction was removed by centrifugation for 40 minutes at 16,000 rpm. The protein was initially purified by affinity chromatography using 5 mL of Ni-NTA resin (Qiagen). The supernatant from the cell lysate was incubated with the Ni-NTA resin for one hour. After washing the bound resin with 40 mL of 50 mmol/L Tris-HCl (pH 8.0), 350 mmol/L NaCl, 40 mmol/L imidazole, and 5 mmol/L β-ME, the protein was eluted in an identical buffer containing 350 mmol/L imidazole. The elution fraction was dialyzed against a buffer containing 30 mmol/L Na_2HPO_4 (pH 6.7), NaCl (150 mmol/L), and DTT (5 mmol/L), and the His-GB1 solubility tag was cleaved using TEV protease. The digested NFATc3 and His-GB1 were separated and further purified using size exclusion chromatography (GE Healthcare Life Sciences "Superdex 75 10/300 GL").

In Vitro *Phosphorylation of NFATc3*

NMR experiments were performed on a Varian (Agilent DD2 700) spectrometer equipped with a cryogenically cooled probe, and the spectrum was recorded at 287 K. CDK4/cyclin D1 and CDK6/cyclin D3 kinases were purchased from Signalchem. The phosphorylation reaction was performed with a sample containing 0.1 mmol/L ^{15}N-labeled NFATc3 with the addition of 10 μg CDK4 or 10 μg CDK6 in kinase reaction buffer [50 mmol/L MES (pH 6.7), 140 mmol/L NaCl, 10 mmol/L $MgCl_2$, 0.1 mmol/L EDTA, 2 mmol/L ATP and 5 mmol/L DTT]. First, a control experiment of unphosphorylated NFATc3 in same kinase reaction buffer was recorded, followed by addition of kinases and phosphorylation was monitored by using 2-D ^{15}N-HSQC experiments. In the inhibition assay, approximately 0.7 μmol/L of CKD6 was preincubated with 7 μmol/L inhibitor before addition to ^{15}N-labeled NFATc3 sample. Here, 2.5 μL of a 1 mmol/L stock of the inhibitor was added to 350 μL of the NMR sample. In a control experiment, the same amount of DMSO (2.5 μL) was added. All spectra were processed using nmrPipe and analyzed with CcpNmr-Analysis (version 2.4.1).

Western Blots and Antibodies

Cells were lysed in M-PER buffer (Thermo Scientific) containing protease/phosphatase inhibitor cocktail (Roche). Protein concentration was measured using a BCA assay (Pierce). Equivalent amounts of each sample were loaded on 4%–12% Bis-Tris gels (Invitrogen), transferred to nitrocellulose membranes, and immunoblotted with antibodies against CDK4, CDK6, β-catenin, active β-catenin, phospho-S536-p65, total p65, and Actin (Cell Signaling Technology), pS172-NFAT2 (R&D Systems), and NFAT2 (Invitrogen). IRDye 800–labeled goat anti-rabbit IgG and IRDye 680–labeled goat anti-mouse IgG secondary antibodies were purchased from LI-COR Biosciences, and membranes were detected on an Odyssey detection system (LI-COR Biosciences).

Animal Studies

All animal studies were reviewed and approved by the Institutional Animal Care and Use Committee (IACUC) at DFCI (Boston, MA). The GEMM harboring a conditional activating mutation of endogenous *Kras* ($Kras^{LSL\text{-}G12D/+}$) crossed with p53 conditional knockout $Trp53^{fl/fl}$ has been described previously (36). CRE recombinase was induced through intranasal inhalation of 5×10^6 p.f.u. adeno-Cre (University of Iowa adenoviral core).

For drug treatment studies in GEMMs, mice were evaluated by MRI imaging to quantify lung tumor burden before and after drug treatment. Mice were treated with either vehicle, 100 mg/kg trilaciclib, or 100 mg/kg palbociclib daily by oral gavage.

For allograft studies, lung tumor nodules were isolated from $Kras^{LSL\text{-}G12D}Trp53^{fl/fl}$ mice (C57BL/6 background), minced into small pieces, and plated onto tissue culture plates and passaged at least 5 times before implantation into mice.

For syngeneic models, MC38 and CT26 cells were injected into 6–8-week-old C57BL/6 or BALB/c female mice subcutaneously, respectively. Vehicle control, CDK4/6 inhibitors (trilaciclib or palbociclib) were treated alone or together with PD-1 antibody starting at the indicated time point, using an intermittent dosing schedule of 3 days on, 4 days off until experimental endpoint.

PD-1 antibody was administered three times a week (Monday, Wednesday, and Friday) at 200 μg/mouse through an intraperitoneal injection.

Patient Samples

Samples from human subjects treated at Massachusetts General Hospital and DFCI were assembled for PDOTS profiling and culture between June and October 2016. Studies were conducted according to the Declaration of Helsinki and informed consent was obtained from all subjects. Tumor samples were collected and analyzed according to Dana-Farber/Harvard Cancer Center IRB-approved protocols.

Flow Antibodies

Lung-infiltrating immune cells were stained with different combinations of fluorochrome-coupled antibodies against mouse CD45 (clone 30-F11, BioLegend), CD3 (clone 17A2, BioLegend), CD4 (clone GK1.5, BioLegend), CD8 (clone 53-6.7, BioLegend), CD11b (clone M1/70, BioLegend), CD11c (clone N418, BioLegend), FOXP3 (clone FJK-16s, eBioscience), CD279 (PD-1, clone 29F.1A12, BioLegend), CD152 (CTLA4, clone UC10-4B9, eBioscience), TIM3 (clone RMT3-23, eBioscience), CD223 (LAG3, clone C9B7W, BioLegend), IL2 (clone JES6-5H4, BioLegend), IFNγ (clone XMG1.2, BioLegend), BrdUrd (clone Bu20a, BioLegend). Jurkat, PD-1–Jurkat, and human PBMCs were stained with fluorochrome-coupled antibodies against human CD3 (clone HIT3a, BioLegend), CD4 (clone OKT4, BioLegend), and CD279 (PD-1, clone EH12.2H7, BioLegend).

MRI Quantification

Animals were anesthetized with isoflurane to perform MRI of the lung field using BioSpec USR70/30 horizontal bore system (Bruker) to scan 24 consecutive sections. Tumor volumes within the whole lung were quantified using 3-D slicer software to reconstruct MRI volumetric measurements as described previously (36). Acquisition of the MRI signal was adapted according to cardiac and respiratory cycles to minimize motion effects during imaging.

Spheroid Preparation and Microfluidic Culture

Experiments were performed as described previously (28). Briefly, fresh tumor specimens from human patients were received in media (DMEM) on ice and minced in 10-cm dishes (on ice) in a sterile field. S2 fractions (40–100 μm) were used for *ex vivo* culture as described previously (28). An aliquot of the S2 fraction was pelleted and resuspended in type I rat tail collagen (Corning) and the spheroid–collagen mixture was then injected into the center gel region of the 3-D microfluidic culture device. After 30 minutes at 37°C, collagen hydrogels containing PDOTS/MDOTS were hydrated with media with indicated treatments. MDOTS were treated with IgG isotype control (10 μg/mL, clone 2A3) or rat-α-mouse anti–PD-1 (10 μg/mL, clone RMP1-14, BioXCell). Both MDOTS and PDOTS were treated with vehicle (DMSO), palbociclib (palb; 100 nmol/L), or trilaciclib (100 nmol/L).

Live/Dead Staining

Dual labeling was performed by loading microfluidic device with Nexcelom ViaStain AO/PI Staining Solution (Nexcelom, CS2-0106). Following incubation with the dyes (20 minutes at room temperature in the dark), images were captured on a Nikon Eclipse 80i fluorescence microscope equipped with Z-stack (Prior) and CoolSNAP CCD camera (Roper Scientific). Image capture and analysis was performed using NIS-Elements AR software package. Whole device images were achieved by stitching in multiple captures. Live and dead cell quantification was performed by measuring total cell area of each dye.

Cytokine Profiling Analysis of Murine BAL Fluid

Mouse lung bronchoalveolar lavage (BAL) was performed by intratracheal injection of 2 mL of sterile PBS followed by collection by aspiration. Cytokines were measured using 19-plex mouse magnetic Luminex kit (R&D Systems), Mouse Cytokine 23-plex Assay (Bio-Rad), or Human Cytokine 40-plex Assay (Bio-Rad) and measured on Bio-Plex 200 system (Bio-Rad). Concentrations (pg/mL) of each protein were derived from 5-parameter curve fitting models. Fold changes relative to the control were calculated and plotted as $\log_2$ fold change. Lower and upper limits of quantitation (LLOQ/ULOQ) were derived from standard curves for cytokines above or below detection. Mouse IL6 and IL10 concentrations were further confirmed by ELISA (BioLegend).

Tumor-Infiltrating Immune Cell Isolation and FACS Analysis

Mice were sacrificed, and lungs were perfused using sterile PBS through heart perfusion from the left ventricle after BAL fluid collection. The whole lung was minced into small pieces and digested in collagenase D (Sigma) and DNase I (Sigma) in Hank's Balanced Salt Solution (HBSS) at 37°C for 30 minutes. After incubation, the digested tissue was filtered through a 70-μm cell strainer (Thermo Fisher Scientific) to obtain single-cell suspensions. Separated cells were treated with 1× RBC lysis buffer (BioLegend) to lyse red blood cells. Live cells were determined by LIVE/DEAD fixable aqua dead cell stain kit (Molecular Probes). The cell pellets were resuspended in PBS with 2% FBS for FACS analysis. Cells were stained with cell surface markers as indicated followed by fixation/permeabilization using FOXP3 fixation/permeabilization kit (eBioscience). Cells were imaged on BD LSRFortessa (BD Biosciences) and analyzed using FlowJo software (Tree Star).

Single-Cell RNA-seq

Library preparation and preprocessing. Single-cell suspensions from *Kras*$^{G12D/+}$*Trp53*$^{fl/fl}$ GEMM mice treated with trilaciclib were isolated as described for tumor-infiltrating immune cells, with modifications. After isolation, live cells were stained and sorted for the CD45$^+$CD3$^+$DAPI$^-$ population and plated at one cell/well of a skirted twin.tec 96-well plate (Eppendorf) containing 1× TCL buffer (Qiagen catalog no. 1031576) spiked with ERCC (Ambion, 1:2,000,000 dilution ratio). In total, four 96-well plates were generated, two plates with and two plates without ERCC spike-ins. After sorting, full-length RNA-seq from isolated single cells was performed according to SMART-seq2 protocol with modifications. Briefly, total RNA was purified using RNA-SPRI beads. Poly(A)+ mRNA was converted to cDNA for amplification. The converted cDNA transcript was subject to barcoding specific to each sample using transposon-based fragmentation that used dual indexing. For single-cell sequencing, each cell was given its own combination of barcodes. Barcoded cDNA fragments were then pooled prior to sequencing. Sequencing was carried out as paired-end (PE) 2 × 36 bp with an additional 8 cycles for each index on NexSeq 500 desktop sequencer (Illumina). To obtain quantitative mapping information, PE reads were mapped to the mouse genome (mm9), concatenated with ERCC sequences for spiked-in samples, by STAR (56). Estimated transcript counts and transcripts per million (TPM) for the mouse Gencode vM1 annotation, concatenated with ERCC sequence information for spiked-in samples, were obtained using the pseudo-aligner Kallisto (57). Aggregated and library scaled TPM values for genes were obtained according to the methods described (58) and were used in further downstream differential distribution, GO, and cell-cycle analysis. Only cells that had a minimum of 100,000 PE reads, and with at least 20% alignment to the transcriptome, were retained for further analysis. To further exclude cells that displayed low quality, we collected quality metrics

for library size, library complexity, duplicate reads, and mitochondrial and ribosomal read fraction, and performed principal component analysis (PCA) combined with density-based clustering (dbscan; http://citeseerx.ist.psu.edu/viewdoc/summary?doi=10.1.1.71.1980) to identify and remove outlier cells relative to the largest and homogeneous group of single cells (27 cells removed). Genes were considered not expressed if TPM < 1 and were subsequently removed if not detected in at least 10% of remaining cells.

The single-cell RNA-seq results have been deposited in the National Center for Biotechnology Information's Gene Expression Omnibus and are accessible through GEO Series accession number GSE89477 (https://www.ncbi.nlm.nih.gov/geo/query/acc.cgi?acc= GSE89477).

Single-Cell RNA-seq Analysis

Normalization. We used a multistep approach using the R package SCONE to identify the optimal normalization strategy and account for possible batch effects, observed and hidden technical covariates (59). First, we identified the most stable 200 genes between the two plates that contained spike-ins. Next, these genes were used in the SCONE framework as negative control genes for unwanted variation for all plates. We continued with highest scored normalization strategy according to SCONE metrics, which included adjusting for batch and biological effects, removal of observed technical variation based on previously identified quality metrics, scaling for library size with DESeq, and imputing drop-out events using a combined clustering and probabilistic scoring algorithm.

Cell-cycle classification. To assign cells to a cell-cycle stage, we applied the cyclone classification tool as described previously (60).

Feature selection and cell clustering. To identify the most informative genes for clustering single cells, we continued only with the Gencode defined gene types, protein_coding and lincRNA, which contain most genes and displayed the highest coefficient of variation. Subsequently, we combined two approaches. First, we identified genes that displayed more than expected variance modeled by the relationship between variance and log expression with LOESS. Next, these genes were used to perform PCA, and the 100 most correlated and anticorrelated genes for the first five principal components were retained for reducing dimensionality and separating cells in gene expression space with t-SNE. Distinct groups were identified applying density-based clustering (dbscan) on the t-SNE–generated coordinates, resulting in 3 groups of cells.

Differential distribution and GO analysis. Genes that display differential distribution between previously identified groups or between treatments were discovered by performing pairwise comparisons with the scDD (http://biorxiv.org/content/early/2015/12/29/035501) package in R. Enriched biological processes were identified using the online GOrilla tool (http://bmcbioinformatics.biomedcentral.com/articles/10.1186/1471-2105-10-48).

BrdUrd Incorporation

C57BL/6 mice were subjected to tail-vein injection with the *Kras*$^{G12D/+}$*Trp53*$^{fl/fl}$ (KP) tumor cell line (1×10^6 cells/mouse) to induce orthotopic tumor growth in the lung. Tumor-bearing mice or C57BL/6 background naïve mice were treated with vehicle (10 μL/g), palbociclib (100 mg/kg), or trilaciclib (100 mg/kg) by daily oral gavage for two consecutive days. At day 3, mice received an intraperitoneal injection of BrdUrd (BD Biosciences) at 2 mg/mouse in sterile PBS. Mice were sacrificed 24 hours after BrdUrd injection and splenocytes were isolated and stained for surface markers. Cells were fixed and permeabilized with FOXP3 fixation/permeabilization buffer (eBioscience), followed by DNase I digestion (0.3 mg/mL, Roche) at 37°C for 1 hour. Cells were stained with fluorochrome-conjugated anti-BrdUrd antibody (BioLegend) and analyzed on LSR-Fortessa (BD Biosciences).

Cell Coculture and Cytokine Production

Naïve or KP tumor–bearing C57BL/6 mice were sacrificed and total splenocytes were harvested. Spleens were digested with collagenase D (Roche) and DNase I (Roche) at 37°C for 30 minutes, followed by 1× ACS lysis buffer (BioLegend) incubation to lyse red blood cells. The collected total splenocytes were stained with the fluorochrome-conjugated cell-surface markers CD3, CD4, CD8, and CD25 to isolate different T-cell subpopulations, including conventional T cells Tconv ($CD3^+CD4^+CD25^-$), Treg ($CD3^+CD4^+CD25^+$), and $CD8^+$ ($CD3^+CD8^+$), using BD FACSAria II SORP cell sorter (BD Biosciences). DAPI (4′,6-diamidino-2-phenylindole) staining was used to exclude dead cells. Sorted cells were cultured in 96-well plates precoated with CD3 antibody (eBioscience) and treated with trilaciclib in the presence of CD28 (eBioscience). Cells were collected 3 days after culturing and cytokine production of IFNγ and IL2 was determined by intracellular staining and analyzed on BD LSR-Fortessa (BD Biosciences).

Transient Transfection

siRNA targeting human CDK4 or CDK6 (GE Dharmacon) or constructs for NFAT-Firefly Luciferase or *Renilla* Luciferase-SV40 (Addgene) were electroporated into cells using the Neon transfection system (Invitrogen) according to the manufacturer's protocol.

Quantitative RT-PCR

Total RNA was extracted from cells using TRIzol (Invitrogen), and cDNA was generated using the SuperScript II Reverse Transcriptase Kit (Invitrogen). Quantitative PCR was performed using Power SYBR Green PCR Master Mix (Applied Biosystems), and transcript levels were normalized to Actin. Samples were run in triplicate. Primer sequences are as follows: Forward primer (5′–3′): *IL2*, AACT CACCAGGATGCTCACA; *IL3*, CAACCTCAATGGGGAAGACCA; *GM-CSF*, TGCTGAGATGAATGAAACAGTAGA; Actin, CGCACC ACTGGCATTGTCAT. Reverse primer (5′–3′): *IL2*, TTGCTGAT TAAGTCCCTGGGT; *IL3*, TGGATTGGATGTCGCGTGG; *GM-CSF*, CTGGGTTGCACAGGAAGTT; Actin, TTCTCCTTGATGTCACG CAC.

Luciferase Assay

Luminescence was measured using the Dual-Glo Luciferase Assay System (Promega) from cells transiently transfected with NFAT-Firefly Luciferase and *Renilla* Luciferase-SV40 on a Clariostar Microplate Reader (BMG Labtech). Samples were run in triplicate.

Statistical Analysis

Data are presented as mean with SEM unless otherwise specified. Statistical comparisons were performed using unpaired Student *t* test for two-tailed *P* values unless otherwise specified (*, $P < 0.05$; **, $P < 0.01$; ***, $P < 0.001$).

Disclosure of Potential Conflicts of Interest

J. Deng has ownership interest in a patent application. E.S. Wang has ownership interest in a patent application. R.W. Jenkins has ownership interest in DFCI US patent WO20112172A1. C.P. Paweletz has received speakers' bureau honoraria from AstraZeneca and Bio-Rad. J.E. Bisi has ownership interest (including patents) in G1 Therapeutics. P.J. Roberts has ownership interest (including patents) in G1 Therapeutics. J.C. Strum has ownership interest (including patents) in G1 Therapeutics. R. Bueno reports receiving commercial

research grants from Exosome, Inc., Novartis Institutes for Biomedical Research, HTG Molecular Diagnostics, Inc., Gritstone Oncology, Inc., Genentech, Inc., Verastem, Inc., Siemens, Myriad Genetics, Inc., and Castle Bioscience; has ownership interest (including patents) in Navigation Sciences; is a consultant/advisory board member for Bio-Medical Insights, Inc.; and has provided expert testimony for Arthur Tuverson, LLC, Balick & Balick, LLC, David Weiss, LLC, Morrison Mahoney, Neil Leifer, Esq., Satterly & Kelly, LLC, Rice Dolan & Kershaw, Ferraro Law Firm, and AstraZeneca. G.J. Freeman has received honoraria from the speakers bureaus of MI Bioresearch, Expert Conn, and MPM Capital, and has ownership interest (including patents) in Novartis (all related to licensed patents in the PD-1/PD-L1 field), Roche, Bristol-Myers Squibb, Merck, EMD Serono, AstraZeneca, and Dako. N.E. Sharpless has ownership interest (including patents) in G1 Therapeutics and is a consultant/advisory board member for the same. G.I. Shapiro reports receiving commercial research grants from Pfizer, Lilly, and Merck/EMD Serono and is a consultant/advisory board member for Pfizer, Lilly, G1 Therapeutics, Roche, and Vertex Pharmaceuticals. D.A. Barbie has ownership interest in DFCI US Patent WO2016112172A1 and is a consultant/advisory board member for N of One. K.-K. Wong has ownership interest (including patents) in G1 Therapeutics and is a consultant/advisory board member for the same. No potential conflicts of interest were disclosed by the other authors.

Authors' Contributions

Conception and design: J. Deng, E.S. Wang, R.W. Jenkins, A.R. Aref, J.A. Sorrentino, J.H. Lorch, R. Bueno, G.I. Shapiro, D.A. Barbie, N.S. Gray, K.-K. Wong

Development of methodology: J. Deng, E.S. Wang, R.W. Jenkins, K. Yates, A.R. Aref, E. Ivanova, C.P. Paweletz, M. Bowden, T. Chen, E. Haines, P.J. Roberts, J.H. Lorch, S. Parangi, G.J. Freeman, W.N. Haining, D.A. Barbie, K.-K. Wong

Acquisition of data (provided animals, acquired and managed patients, provided facilities, etc.): J. Deng, E.S. Wang, R.W. Jenkins, S. Li, K. Yates, W. Huang, A.R. Aref, E. Ivanova, M. Bowden, C.W. Zhou, G.S. Herter-Sprie, J.A. Sorrentino, J.E. Bisi, P.H. Lizotte, A.A. Merlino, M.M. Quinn, L.E. Bufe, A. Yang, Y. Zhang, H. Zhang, P. Gao, T. Chen, M.E. Cavanaugh, A.J. Rode, E. Haines, P.J. Roberts, W.G. Richards, J.H. Lorch, V. Gunda, G.M. Boland, R. Bueno, S. Palakurthi, J. Ritz, H. Arthanari, G.I. Shapiro, K.-K. Wong

Analysis and interpretation of data (e.g., statistical analysis, biostatistics, computational analysis): J. Deng, E.S. Wang, R.W. Jenkins, S. Li, R. Dries, K. Yates, H. Liu, A.R. Aref, E. Ivanova, C.P. Paweletz, M. Bowden, C.W. Zhou, G.S. Herter-Sprie, J.A. Sorrentino, P.H. Lizotte, T. Chen, M.E. Cavanaugh, P.J. Roberts, J.C. Strum, J.H. Lorch, S. Palakurthi, J. Ritz, N.E. Sharpless, H. Arthanari, G.I. Shapiro, K.-K. Wong

Writing, review, and/or revision of the manuscript: J. Deng, E.S. Wang, R.W. Jenkins, R. Dries, S. Chhabra, A.R. Aref, E. Ivanova, M. Bowden, G.S. Herter-Sprie, J.A. Sorrentino, J.E. Bisi, M.E. Cavanaugh, P.J. Roberts, J.C. Strum, W.G. Richards, J.H. Lorch, S. Parangi, V. Gunda, G.M. Boland, G.J. Freeman, J. Ritz, W.N. Haining, N.E. Sharpless, G.I. Shapiro, D.A. Barbie, N.S. Gray, K.-K. Wong

Administrative, technical, or material support (i.e., reporting or organizing data, constructing databases): E.S. Wang, A.R. Aref, P. Gao, G.I. Shapiro, N.S. Gray

Study supervision: J. Deng, E.S. Wang, T. Chen, J.H. Lorch, R. Bueno, G.I. Shapiro, D.A. Barbie, N.S. Gray, K.-K. Wong

Other (designed, performed, and analyzed NMR experiments on NFAT): S. Chhabra

Acknowledgments

We thank the Dana-Farber Cancer Institute Animal Resources Facility staff for their support of the animal studies. We would also like to acknowledge the Brigham and Women's Hospital, Dana-Farber Cancer Institute, and Massachusetts General Hospital for providing the patient specimens used in this study. We thank the Broad Institute for facilitating the single-cell sequencing experiment. And finally, we appreciate the generous gift of anti–PD-1 antibody from G.J. Freeman used for the mouse studies. This work was supported by a Damon Runyon Cancer Research Fellowship DRG-2270-16 (to E.S. Wang), CA154303-05 (to N.S. Gray), and CA179483-03 (to N.S. Gray), NIH/NCI P01CA120964 (to K.-K. Wong), 5R01CA163896-04 (to K.-K. Wong), 5R01CA140594-07 (to K.-K. Wong), 5R01CA122794-10 (to K.-K. Wong), and 5R01CA166480-04 (to K.-K. Wong), and funding from a Medical Oncology Discovery grant, Dana-Farber Cancer Institute.

The costs of publication of this article were defrayed in part by the payment of page charges. This article must therefore be hereby marked *advertisement* in accordance with 18 U.S.C. Section 1734 solely to indicate this fact.

Received August 11, 2017; revised October 24, 2017; accepted October 31, 2017; published OnlineFirst November 3, 2017.

REFERENCES

1. Borghaei H, Paz-Ares L, Horn L, Spigel DR, Steins M, Ready NE, et al. Nivolumab versus docetaxel in advanced nonsquamous non-small-cell lung cancer. N Engl J Med 2015;373:1627–39.
2. Robert C, Schachter J, Long GV, Arance A, Grob JJ, Mortier L, et al. Pembrolizumab versus ipilimumab in advanced melanoma. N Engl J Med 2015;372:2521–32.
3. Rizvi NA, Hellmann MD, Snyder A, Kvistborg P, Makarov V, Havel JJ, et al. Cancer immunology. Mutational landscape determines sensitivity to PD-1 blockade in non-small cell lung cancer. Science 2015;348:124–8.
4. Pardoll DM. The blockade of immune checkpoints in cancer immunotherapy. Nat Rev Cancer 2012;12:252–64.
5. Leach DR, Krummel MF, Allison JP. Enhancement of antitumor immunity by CTLA-4 blockade. Science 1996;271:1734–6.
6. Phan GQ, Yang JC, Sherry RM, Hwu P, Topalian SL, Schwartzentruber DJ, et al. Cancer regression and autoimmunity induced by cytotoxic T lymphocyte-associated antigen 4 blockade in patients with metastatic melanoma. Proc Natl Acad Sci U S A 2003;100:8372–7.
7. Nishimura H, Nose M, Hiai H, Minato N, Honjo T. Development of lupus-like autoimmune diseases by disruption of the PD-1 gene encoding an ITIM motif-carrying immunoreceptor. Immunity 1999;11:141–51.
8. Dong H, Strome SE, Salomao DR, Tamura H, Hirano F, Flies DB, et al. Tumor-associated B7-H1 promotes T-cell apoptosis: a potential mechanism of immune evasion. Nat Med 2002;8:793–800.
9. Brahmer JR, Drake CG, Wollner I, Powderly JD, Picus J, Sharfman WH, et al. Phase I study of single-agent anti-programmed death-1 (MDX-1106) in refractory solid tumors: safety, clinical activity, pharmacodynamics, and immunologic correlates. J Clin Oncol 2010;28:3167–75.
10. Sharma P, Allison JP. Immune checkpoint targeting in cancer therapy: toward combination strategies with curative potential. Cell 2015;161:205–14.
11. Mahoney KM, Rennert PD, Freeman GJ. Combination cancer immunotherapy and new immunomodulatory targets. Nat Rev Drug Discov 2015;14:561–84.
12. Kaluza KM, Thompson JM, Kottke TJ, Flynn Gilmer HC, Knutson DL, Vile RG. Adoptive T cell therapy promotes the emergence of genomically altered tumor escape variants. Int J Cancer 2012;131:844–54.
13. Kelderman S, Schumacher TN, Haanen JB. Acquired and intrinsic resistance in cancer immunotherapy. Mol Oncol 2014;8:1132–9.
14. Koyama S, Akbay EA, Li YY, Herter-Sprie GS, Buczkowski KA, Richards WG, et al. Adaptive resistance to therapeutic PD-1 blockade is

associated with upregulation of alternative immune checkpoints. Nat Commun 2016;7:10501.
15. Adams JL, Smothers J, Srinivasan R, Hoos A. Big opportunities for small molecules in immuno-oncology. Nat Rev Drug Discov 2015;14:603–22.
16. Sullivan RJ, Lorusso PM, Flaherty KT. The intersection of immune-directed and molecularly targeted therapy in advanced melanoma: where we have been, are, and will be. Clin Cancer Res 2013;19:5283–91.
17. Akbay EA, Koyama S, Carretero J, Altabef A, Tchaicha JH, Christensen CL, et al. Activation of the PD-1 pathway contributes to immune escape in EGFR-driven lung tumors. Cancer Discov 2013;3:1355–63.
18. Ebert PJ, Cheung J, Yang Y, McNamara E, Hong R, Moskalenko M, et al. MAP kinase inhibition promotes T cell and anti-tumor activity in combination with PD-L1 checkpoint blockade. Immunity 2016;44:609–21.
19. Wells AD, Morawski PA. New roles for cyclin-dependent kinases in T cell biology: linking cell division and differentiation. Nat Rev Immunol 2014;14:261–70.
20. Scheicher R, Hoelbl-Kovacic A, Bellutti F, Tigan AS, Prchal-Murphy M, Heller G, et al. CDK6 as a key regulator of hematopoietic and leukemic stem cell activation. Blood 2015;125:90–101.
21. Min IM, Pietramaggiori G, Kim FS, Passegue E, Stevenson KE, Wagers AJ. The transcription factor EGR1 controls both the proliferation and localization of hematopoietic stem cells. Cell Stem Cell 2008;2:380–91.
22. Macian F. NFAT proteins: key regulators of T-cell development and function. Nat Rev Immunol 2005;5:472–84.
23. Quigley M, Pereyra F, Nilsson B, Porichis F, Fonseca C, Eichbaum Q, et al. Transcriptional analysis of HIV-specific CD8+ T cells shows that PD-1 inhibits T cell function by upregulating BATF. Nat Med 2010;16:1147–51.
24. Garcia CA, Benakanakere MR, Alard P, Kosiewicz MM, Kinane DF, Martin M. Antigenic experience dictates functional role of glycogen synthase kinase-3 in human CD4+ T cell responses. J Immunol 2008;181:8363–71.
25. Ohteki T, Parsons M, Zakarian A, Jones RG, Nguyen LT, Woodgett JR, et al. Negative regulation of T cell proliferation and interleukin 2 production by the serine threonine kinase GSK-3. J Exp Med 2000;192:99–104.
26. Bisi JE, Sorrentino JA, Roberts PJ, Tavares FX, Strum JC. Preclinical characterization of G1T28: a novel CDK4/6 inhibitor for reduction of chemotherapy-induced myelosuppression. Mol Cancer Ther 2016;15:783–93.
27. He S, Roberts PJ, Sorrentino JA, Bisi JE, Storrie-White H, Tiessen RG, et al. Transient CDK4/6 inhibition protects hematopoietic stem cells from chemotherapy-induced exhaustion. Sci Transl Med 2017;9:pii:eaal3986.
28. Jenkins RW, Aref AR, Lizotte PH, Ivanova E, Stinson S, Zhou CW, et al. Ex vivo profiling of PD-1 blockade using organotypic tumor spheroids. Cancer Discov 2018;8:196–215.
29. Veinotte L, Gebremeskel S, Johnston B. CXCL16-positive dendritic cells enhance invariant natural killer T cell-dependent IFNgamma production and tumor control. Oncoimmunology 2016;5:e1160979.
30. Peng D, Kryczek I, Nagarsheth N, Zhao L, Wei S, Wang W, et al. Epigenetic silencing of TH1-type chemokines shapes tumour immunity and immunotherapy. Nature 2015;527:249–53.
31. Anders L, Ke N, Hydbring P, Choi YJ, Widlund HR, Chick JM, et al. A systematic screen for CDK4/6 substrates links FOXM1 phosphorylation to senescence suppression in cancer cells. Cancer Cell 2011;20:620–34.
32. Bienkiewicz EA, Lumb KJ. Random-coil chemical shifts of phosphorylated amino acids. J Biomol NMR 1999;15:203–6.
33. Tholey A, Lindemann A, Kinzel V, Reed J. Direct effects of phosphorylation on the preferred backbone conformation of peptides: a nuclear magnetic resonance study. Biophys J 1999;76:76–87.
34. Porter CM, Havens MA, Clipstone NA. Identification of amino acid residues and protein kinases involved in the regulation of NFATc subcellular localization. J Biol Chem 2000;275:3543–51.
35. Macian F, Garcia-Rodriguez C, Rao A. Gene expression elicited by NFAT in the presence or absence of cooperative recruitment of Fos and Jun. EMBO J 2000;19:4783–95.
36. Chen Z, Cheng K, Walton Z, Wang Y, Ebi H, Shimamura T, et al. A murine lung cancer co-clinical trial identifies genetic modifiers of therapeutic response. Nature 2012;483:613–7.
37. Asghar U, Witkiewicz AK, Turner NC, Knudsen ES. The history and future of targeting cyclin-dependent kinases in cancer therapy. Nat Rev Drug Discov 2015;14:130–46.
38. Chang JT, Ciocca ML, Kinjyo I, Palanivel VR, McClurkin CE, Dejong CS, et al. Asymmetric proteasome segregation as a mechanism for unequal partitioning of the transcription factor T-bet during T lymphocyte division. Immunity 2011;34:492–504.
39. Denkert C, Loibl S, Noske A, Roller M, Muller BM, Komor M, et al. Tumor-associated lymphocytes as an independent predictor of response to neoadjuvant chemotherapy in breast cancer. J Clin Oncol 2010;28:105–13.
40. Balkwill FR, Mantovani A. Cancer-related inflammation: common themes and therapeutic opportunities. Semin Cancer Biol 2012;22:33–40.
41. Grivennikov S, Karin E, Terzic J, Mucida D, Yu GY, Vallabhapurapu S, et al. IL-6 and Stat3 are required for survival of intestinal epithelial cells and development of colitis-associated cancer. Cancer Cell 2009;15:103–13.
42. Crawford A, Angelosanto JM, Kao C, Doering TA, Odorizzi PM, Barnett BE, et al. Molecular and transcriptional basis of CD4(+) T cell dysfunction during chronic infection. Immunity 2014;40:289–302.
43. Puyol M, Martin A, Dubus P, Mulero F, Pizcueta P, Khan G, et al. A synthetic lethal interaction between K-Ras oncogenes and Cdk4 unveils a therapeutic strategy for non-small cell lung carcinoma. Cancer Cell 2010;18:63–73.
44. Schumacher TN, Schreiber RD. Neoantigens in cancer immunotherapy. Science 2015;348:69–74.
45. McFadden DG, Politi K, Bhutkar A, Chen FK, Song X, Pirun M, et al. Mutational landscape of EGFR-, MYC-, and Kras-driven genetically engineered mouse models of lung adenocarcinoma. Proc Natl Acad Sci U S A 2016;113:E6409–17.
46. Ngiow SF, Young A, Jacquelot N, Yamazaki T, Enot D, Zitvogel L, et al. A threshold level of intratumor CD8+ T-cell PD1 expression dictates therapeutic response to anti-PD1. Cancer Res 2015;75:3800–11.
47. Duraiswamy J, Kaluza KM, Freeman GJ, Coukos G. Dual blockade of PD-1 and CTLA-4 combined with tumor vaccine effectively restores T-cell rejection function in tumors. Cancer Res 2013;73:3591–603.
48. De Simone M, Arrigoni A, Rossetti G, Gruarin P, Ranzani V, Politano C, et al. Transcriptional landscape of human tissue lymphocytes unveils uniqueness of tumor-infiltrating T regulatory cells. Immunity 2016;45:1135–47.
49. Kollmann K, Heller G, Schneckenleithner C, Warsch W, Scheicher R, Ott RG, et al. A kinase-independent function of CDK6 links the cell cycle to tumor angiogenesis. Cancer Cell 2016;30:359–60.
50. Handschick K, Beuerlein K, Jurida L, Bartkuhn M, Muller H, Soelch J, et al. Cyclin-dependent kinase 6 is a chromatin-bound cofactor for NF-kappaB-dependent gene expression. Mol Cell 2014;53:193–208.
51. Buss H, Handschick K, Jurrmann N, Pekkonen P, Beuerlein K, Muller H, et al. Cyclin-dependent kinase 6 phosphorylates NF-kappaB P65 at serine 536 and contributes to the regulation of inflammatory gene expression. PLoS One 2012;7:e51847.
52. Martinez GJ, Pereira RM, Aijo T, Kim EY, Marangoni F, Pipkin ME, et al. The transcription factor NFAT promotes exhaustion of activated CD8(+) T cells. Immunity 2015;42:265–78.
53. Infante JR, Cassier PA, Gerecitano JF, Witteveen PO, Chugh R, Ribrag V, et al. A phase I study of the cyclin-dependent kinase 4/6 inhibitor ribociclib (LEE011) in patients with advanced solid tumors and lymphomas. Clin Cancer Res 2016;22:5696–705.

54. Cadoo KA, Gucalp A, Traina TA. Palbociclib: an evidence-based review of its potential in the treatment of breast cancer. Breast Cancer 2014;6:123–33.
55. Fabian MA, Biggs WH III, Treiber DK, Atteridge CE, Azimioara MD, Benedetti MG, et al. A small molecule-kinase interaction map for clinical kinase inhibitors. Nat Biotechnol 2005;23:329–36.
56. Dobin A, Davis CA, Schlesinger F, Drenkow J, Zaleski C, Jha S, et al. STAR: ultrafast universal RNA-seq aligner. Bioinformatics 2013;29:15–21.
57. Bray NL, Pimentel H, Melsted P, Pachter L. Near-optimal probabilistic RNA-seq quantification. Nat Biotechnol 2016;34:525–7.
58. Soneson C, Love MI, Robinson MD. Differential analyses for RNA-seq: transcript-level estimates improve gene-level inferences. F1000Research 2015;4:1521.
59. Risso D, Ngai J, Speed TP, Dudoit S. Normalization of RNA-seq data using factor analysis of control genes or samples. Nat Biotechnol 2014;32:896–902.
60. Scialdone A, Natarajan KN, Saraiva LR, Proserpio V, Teichmann SA, Stegle O, et al. Computational assignment of cell-cycle stage from single-cell transcriptome data. Methods 2015;85:54–61.